Amplitude Versus Offset Analysis For Reservoir Characterization Of A W-Field, Onshore , Niger Delta.

Christopher E. Okon[1] Christopher A. Jackson [2] and Reuben G. Samuel [3]

[1]Department of Geology, University of Calabar, Nigeria.
[2] PetroVision Energy Nigeria Limited, Lagos, Nigeria.
[3] Department of Physics, University of Port Harcourt, Nigeria

ABSTRACT

The amplitude versus offset (AVO) analysis was done to characterized the reservoirs. This study was carried out within the onshore, central swamp, Depobelt east of Niger Delta. This work was to further aid in oilfield development which were the use of well log interpretation to identify permeable reservoir zones and properties, AVO analysis of brine and gas saturation, to estimate primary wave velocity for AVO attributes generation, discrimination of gas reservoir from background lithology, detection of reservoir boundaries, identification of direct hydrocarbon indicators. The techniques adopted were AVO attributes calculation, well-log rock attribute estimation, incident angle and offsets distance extraction, shear and compressional acoustic impedances determination, estimation of bulk and shear moduli of elastic material, permeability and water saturation estimation. The result shows the offset for far, near and full corresponding to the incident angle. The interpreted AVO attributes shows bright and flat spot indicating areas of pronounce amplitude, penetrated by well-02. The plots of amplitude versus offset shows that amplitude decreases as offset angle increases at certain intervals which were selected as shale saturated with gas sand boundary, shale saturated with oil sand and shale saturated with brine sand boundary and amplitudes at different offsets. AVO class 3 observed in intervals 2100 and 2200 ms. The rigidity of sandstone and shale were determined using mu-Rho ($\mu\rho$) and V_P/V_S .Indication of high $\mu\rho$ and low V_P/V_S of 1.8 presented itself as gas sand and higher V_P/V_S from 1.8 to 2.4 indicated shale. Sand found to have low water saturation values between 0.0-0.20 while shale had higher water saturation on the range of 0.22-0.50 indicating poorly consolidated sediments. Fluid contact and sand quality were found using density (ρ) ,μ and λ using well logs applying parameter like Mu-Rho ($\mu\rho$) called rigidity and Lamda-Rho ($\lambda\rho$) called incompressibility.

Main Body Of The Work entitled: Amplitude Versus Offset Analysis For Reservoir Characterization Of 'W-Field', Onshore, Niger Delta.

INTRODUCTION

Introduction

The Niger Delta, seen as one of the highly endowed hydrocarbon province in the earth is situated at the northeastern margin of the gulf of Guinea .The basin is endowed with the sediment influx which covers an area of $75{,}000km^2$ with an average of 12 km thick sediment mostly in the central part (Reijers,1996).Estimated recoverable hydrocarbons for this delta spans about 20 billion barrels of oil and 30 trillion cubic feet of gas . This basin is characterized by the highest petroleum per unit volume of basin fill (Evamy et al.,1978). The Delta is ranked among the world's outstanding prolific petroleum producing Tertiary deltas that accounts for 5% of the world's oil and gas reserves forming about 2.5% of the present–day basin areas of the earth (Reijers,1996). The Niger –Benue present –day drainage area is of about 1,200,000km^{2}and has given rise to a delta area of 75,000km^2, predominantly filled with clastics of about 12,000m found in West Africa, the largest in Africa. Amplitude–versus–offset (AVO) analysis is a tool in characterizing reservoir whose validity not only depends on the Seismic data quality recorded but also on the steps adopted in data processing and the know-how of rock properties. The amplitude character of seismic reflections varies with offset, this depends on the changes in the angle-of- incidence as shown in CMP gathers (pre-stack). Normal angle stack and seismic section (time migrated). Although AVO modeling correlates rock properties to amplitude behavior (offset-dependent) it remains a technique which aid in data processing, interpretation and calibration.

The first work related to the use of AVO dated back since 1900.The basic AVO theory were emphasized by Knott and Zoeppritz in 1899 and 1919 respectively. They

developed equations for plane–wave reflection amplitude as a function of incident angle. Further studies were carried out in later years. The simplification of Zoeppritz equation made it easy for seismic reflection (amplitudes) understanding tied to angle of incidence and physical parameters as opined by Bortfeld (1961). The linkage between AVO to variation of poisson's ratio across contrasting interface was put forward by Koefoed (1955). His findings emphasized the use of Zoeppritz algorithm. Rosa (1976) and Shuey (1985) remarkably had a breakthrough based on their research whose findings predicted lithology using AVO approach.

However, the technique for validating Seismic amplitude anomalies was proposed by Ostrander (1982). This was associated with gas sands which produces amplitude anomalies having impedance contrast less than that of encasing shales, thus the reflection increases in proportion with offset. The associated gas sands remain the largest portion of AVO analysis carried out in the Industry today. Explorationists have learnt over the years that AVO analysis, remains possible in gas sands- reflections and its reflection not directly link to bright spots in a given stacked Seismic data. Classes of AVO span from the range of its effects which are linked with gas sands usually encountered in exploration. These classes are Class 1(high–impedance sands), Class 2 : near-normal incidence (near normal impedance difference sands) and Class 3 (low–acoustic impedance sands). They are also based on the type of anomalies; Class 1: dim out anomalies; Class 2: phase reversal anomalies and Class 3: bright spot anomalies (Rutherford & Williams, 1989).

Methods of AVO analysis includes Identification of permeable reservoir zones and estimation of reservoir properties, AVO analysis of brine and gas saturation, estimation of primary wave for AVO attributes calculation, discrimination of gas reservoir from background lithologies, detect reservoir boundaries,. identify direct

hydrocarbon indicators, Quantify by characterizing reservoir properties in lithology determination.

The area under investigation is located within the onshore portion of the east of the middle swamp Depobelt of the Niger Delta (figure 1) which is located on the margin (continental) , Gulf of Guinea, Equatorial region of West Africa on Longitude $6^0 58^I 23^{II}$E - $7^0 15^I 12^{11}$E, latitudes $4^0 58^I 0^{II}$N - $4^0 54^I 26^{II}$N (Figure 1 and 2) opined by Ehinola & Ejeh (2009).

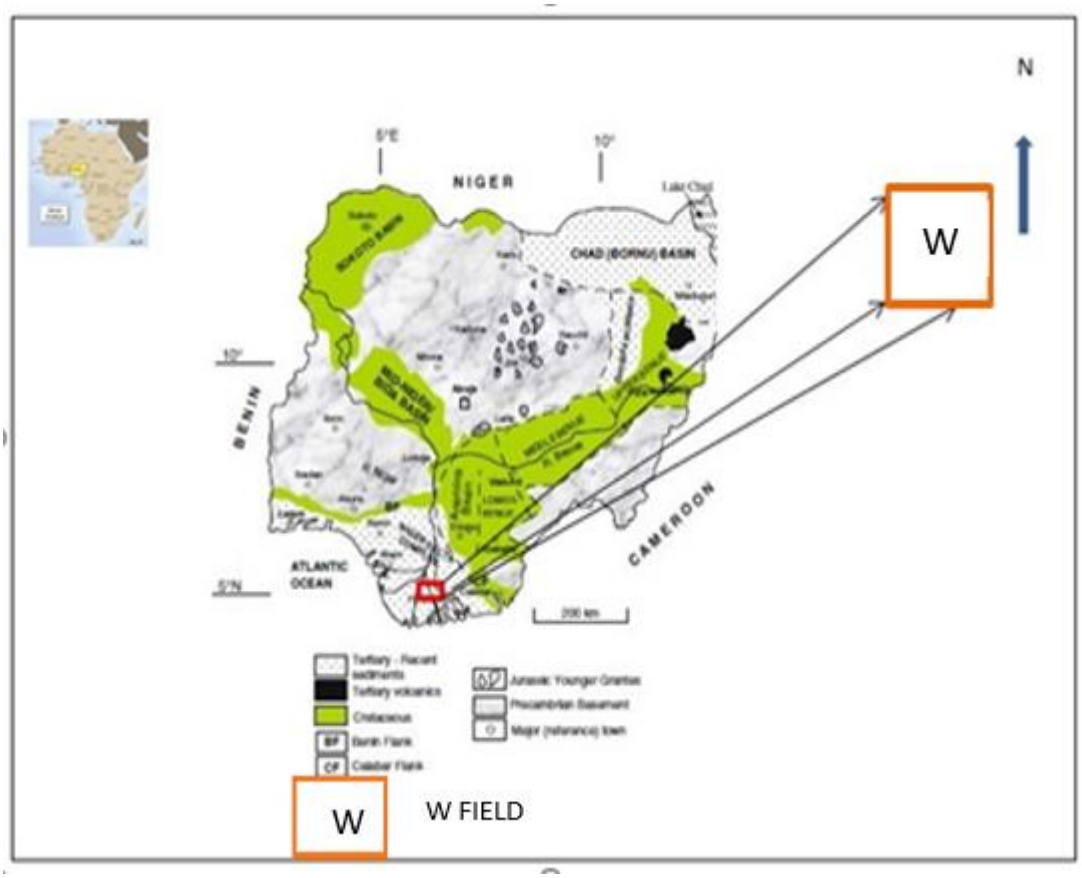

FIG.1a Map of Nigeria showing W - Field location to other major Sedimentary Basins.

(SPDC)

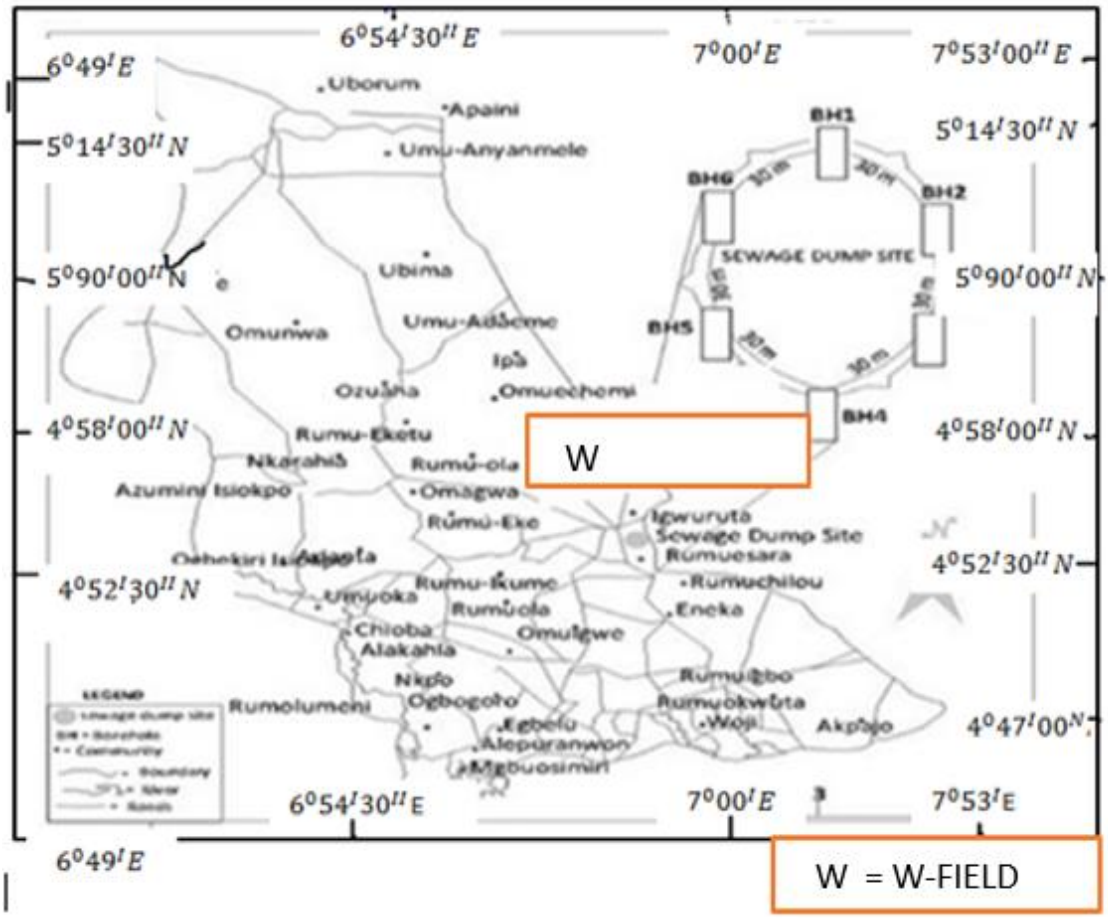

FIG.2. Map showing the Field Area named' W - Field' as it relates to other oil fields

In the bid to solving the problem of oil and gas prospecting, the explorationists are exposed to the challenge of a good reservoir characterization technique. Essentially there are problems of Identifying permeable reservoir zones and estimating the reservoir properties, AVO analysis of brine and gas saturation, estimating primary wave velocity from AVO attribute, discriminating gas reservoir from background lithology, fluid contact detection . Acoustic impedance and shear impedance crossplots serves as a problem in discrimination of fluids in the lithology, use of AVO attributes in detecting reservoir boundaries, identification of direct hydrocarbon indicators as a pointer to detecting presence of hydrocarbon and quantification of reservoir properties in lithology determination. All these constitute problems.

The main target of this work shall be to characterize reservoirs using amplitude versus offset (AVO) as a tool in a field area, Niger Delta. The specific objectives of this study are to: Identify permeable reservoir zone and estimate the reservoir properties, AVO analysis of brine and gas saturation, Estimate primary wave for AVO attributes ,Discriminate gas reservoir from background lithology ,Detect reservoir boundaries. Identify direct hydrocarbon indicators, Quantify characterization of properties of the reservoir in lithology determination. The basic interest of this work shall be focus on characterization of reservoir using amplitude versus offset technique. The estimation of reservoir properties, detection of water saturation ,estimation of primary wave velocity ,discrimination of gas reservoir , mapping of reservoir boundaries, identification of direct hydrocarbon indicators and crossplots of reservoir properties for further characterization .

Reflection coefficient classification put forward by Rutherford and Williams (1989) based on curves now becomes an industrial standard now referred to as bright

spot, phase reversal and dim out. This lead to classes on the basis of plots of amplitude versus offset into class 1,2 and 3 .(Figure 3).

Based on this , the slope for the plot of amplitude versus offset is negative for all classes , amplitude decreases with incident angle as shown in class 2 and 3 (interpreted as gas saturated amplitude decreases with source-receiver distance (Castagna & Swan, 1998), this was named class 4 anomalies being a large amplitude link with the hydrocarbons.

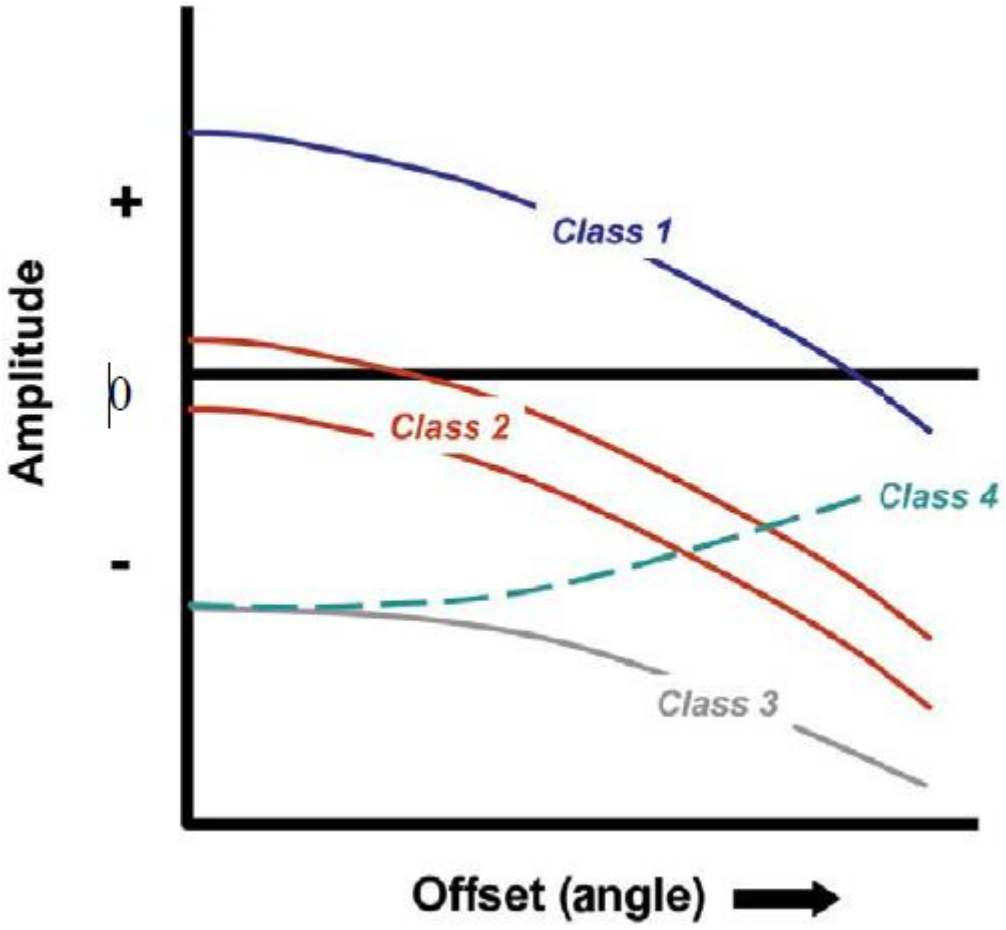

FIG.3:Plot of Angle of Incidence versus Reflection Coefficient
(Source: Hong *et al.*,2006)

MATERIALS AND METHODS

Materials

The materials available for this work was 3D seismic data (in SEG-Y format) , Hampson Russell , RokDoc and Interactive petrophysics software installed in a personal laptop, checkshot data , suites of wireline in LAS format (sonic, resistivity, gamma ray , density , neutron and SP), Pre-stack seismic data (depth migrated) .

Well log data

The log data available for this work was made available by Shell Petroleum Development Company (SPDC) . It was confirmed after successful loading into the software that this logs were given from seven wells. Some of its were reasonably fewer , however about three of the wells had complete log signatures.

Upon successful loading of the load data , the base map of the study area was display (Figure 4) Wells situated in North Eastern part of the Field as generated after loading the data in the HRS software. We show the 3 D view of study area (Figure 5). Note only two wells contains somewhat complete suite of logs ,hence highly useful for this work.

From the table 1, Well-02 and -06 were identified with a complete suite of good quality logs that sampled all or most of the logging types, lithologies and some of its logs are further displayed in figure 6 and 7 . The sonic data were calibrated with the checkshot data, the numbering of the tracks is done from left to right. .

Density and Resistivity are in track 3 and 4, respectively. The gamma ray log , Caliper, V_p curves are in tracks 1, 2 and 5 respectively. The measured depth calibrated to the right and the two way travel time calibrated to the left. The caliper log shows stable borehole conditions.

The wireline log data were from seven wells (labeled 01,02,03,04, 05,06,07) loaded in software namely,'' Hampson Russell, RokDoc and Interactive Petrophysics'' these data were adequately quality controlled and adjusted.

To accomplish this research work the following workflow was adopted (Figure 8)

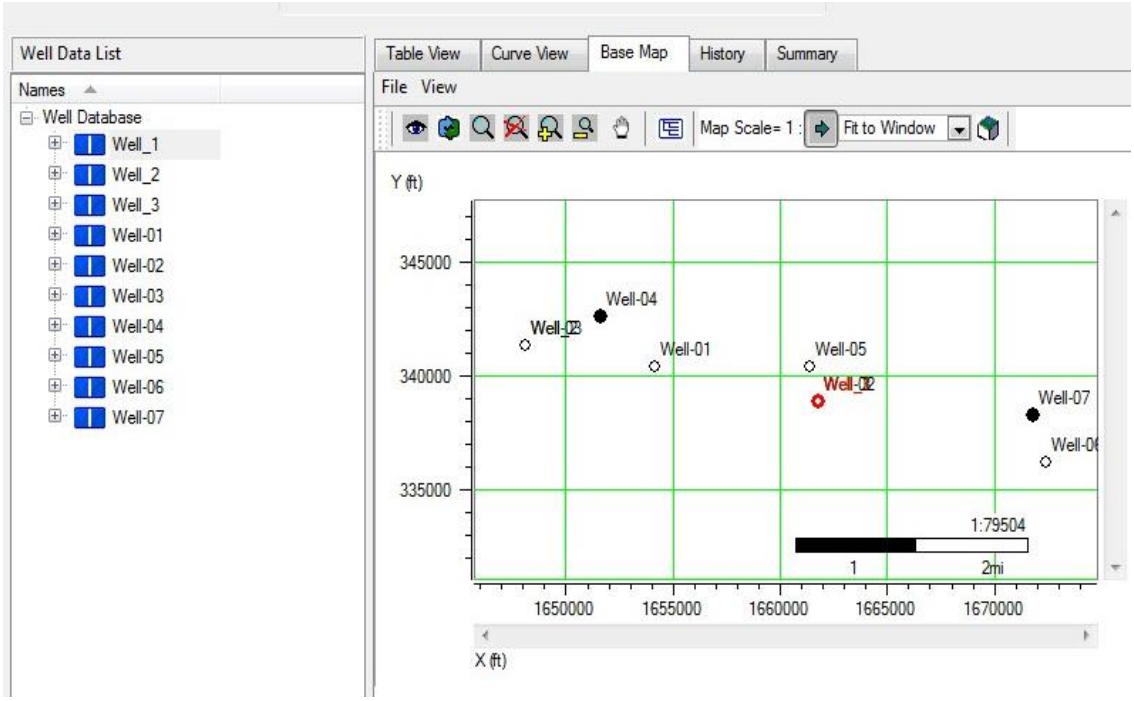

FIG.4: The base Map indicating wells locations in 2-D.

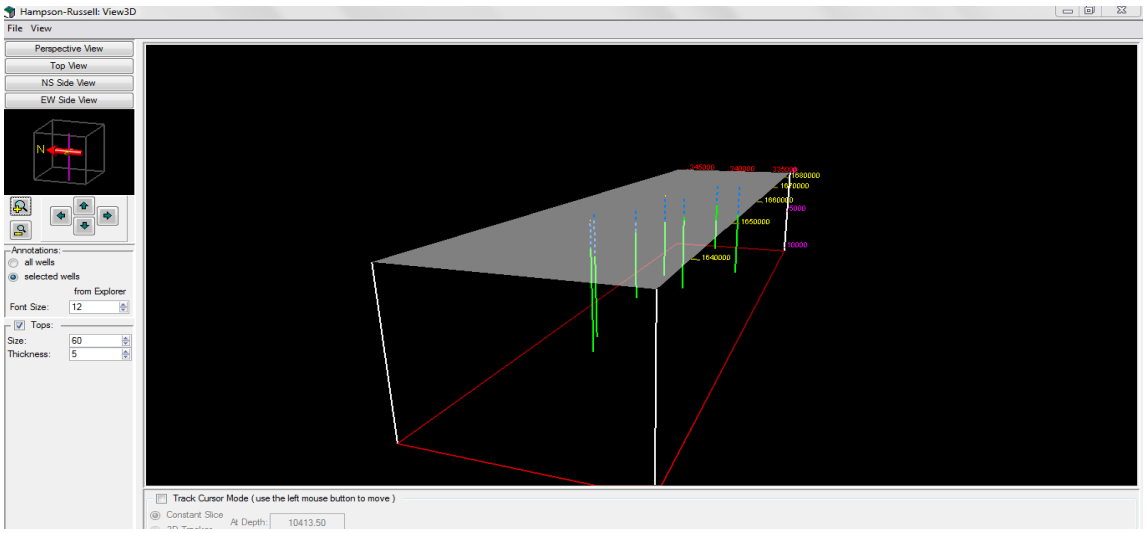

FIG.5 : 3-dimensional display of wells showing area under investigation (study area).

Table 1: Showing suites of logs available in each wells

WELL	GR (API)	CALLIPER (INCHES)	RESIS. (Ωm)	P-WAVES	DEN. (g/cm^3)	PRESS.(Psi)	CHECK SHOT (ms)	SP	NEUTRON – POROSITY
Well-01	Yes	Yes	Yes	Yes	No	No	No	No	No
Well-02	Yes	Yes	Yes	Yes	Yes	Yes	Yes	Yes	Yes
Well-03	Yes	No	Yes	No	No	No	No	No	No
Well-04	Yes	No	Yes	No	Yes	No	No	Yes	No
Well-05	Yes	No	Yes	No	Yes	No	No	Yes	No
Well-06	Yes	Yes	Yes	Yes	Yes	Yes	No	Yes	Yes
Well-07	Yes	No	Yes	Yes	Yes	No	No	Yes	Yes

GR - gamma ray
RESIS - resistivity
DEN -density
PRESS - pressure
SP- spontaneous potential

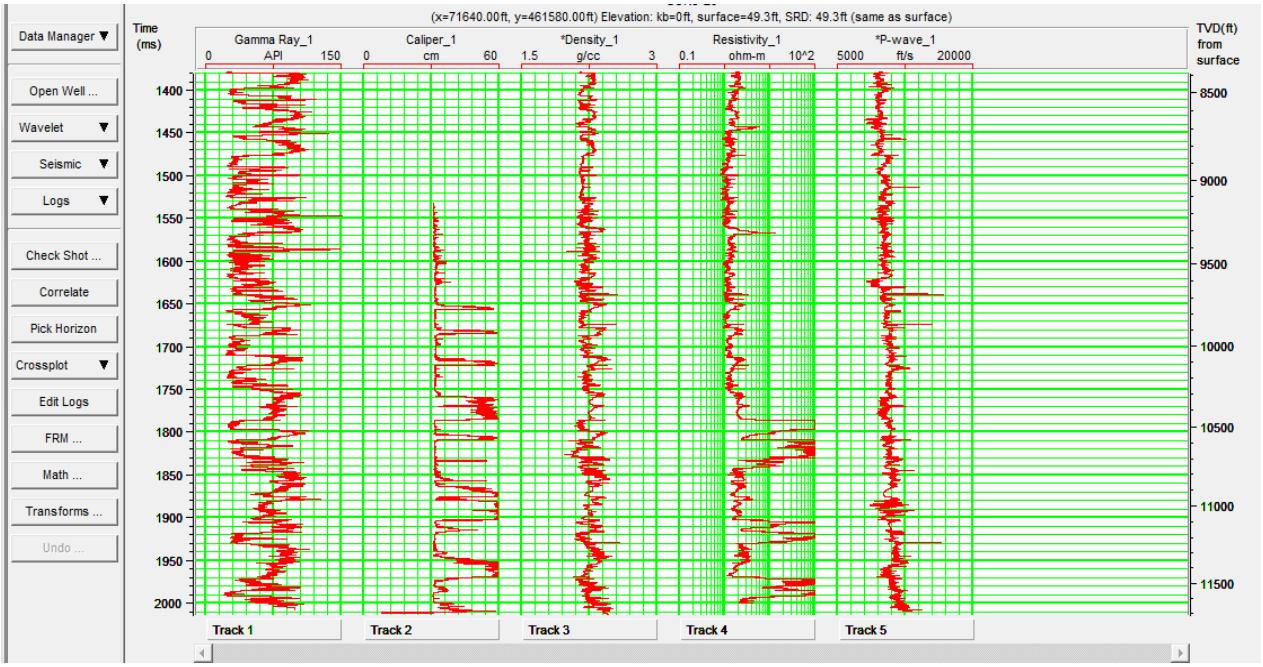

FIG.6:Wireline Log data (suite) displaying signatures representingwell-02.The depth column (TVD) in feet shown on the right hand side while the time column also shows on the left hand side.

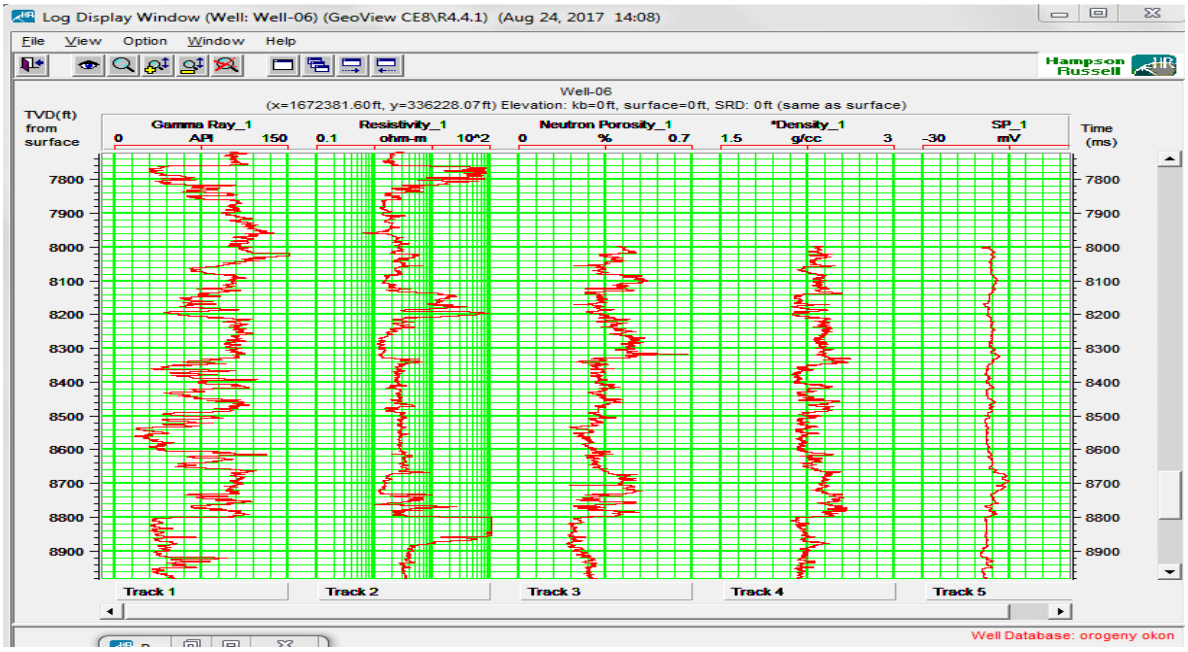

FIG.7: Wireline log (suite) displaying signatures representing well-06.
The depth column (TVD) in feet shown on the right hand side while the time column also shows on the left hand side.

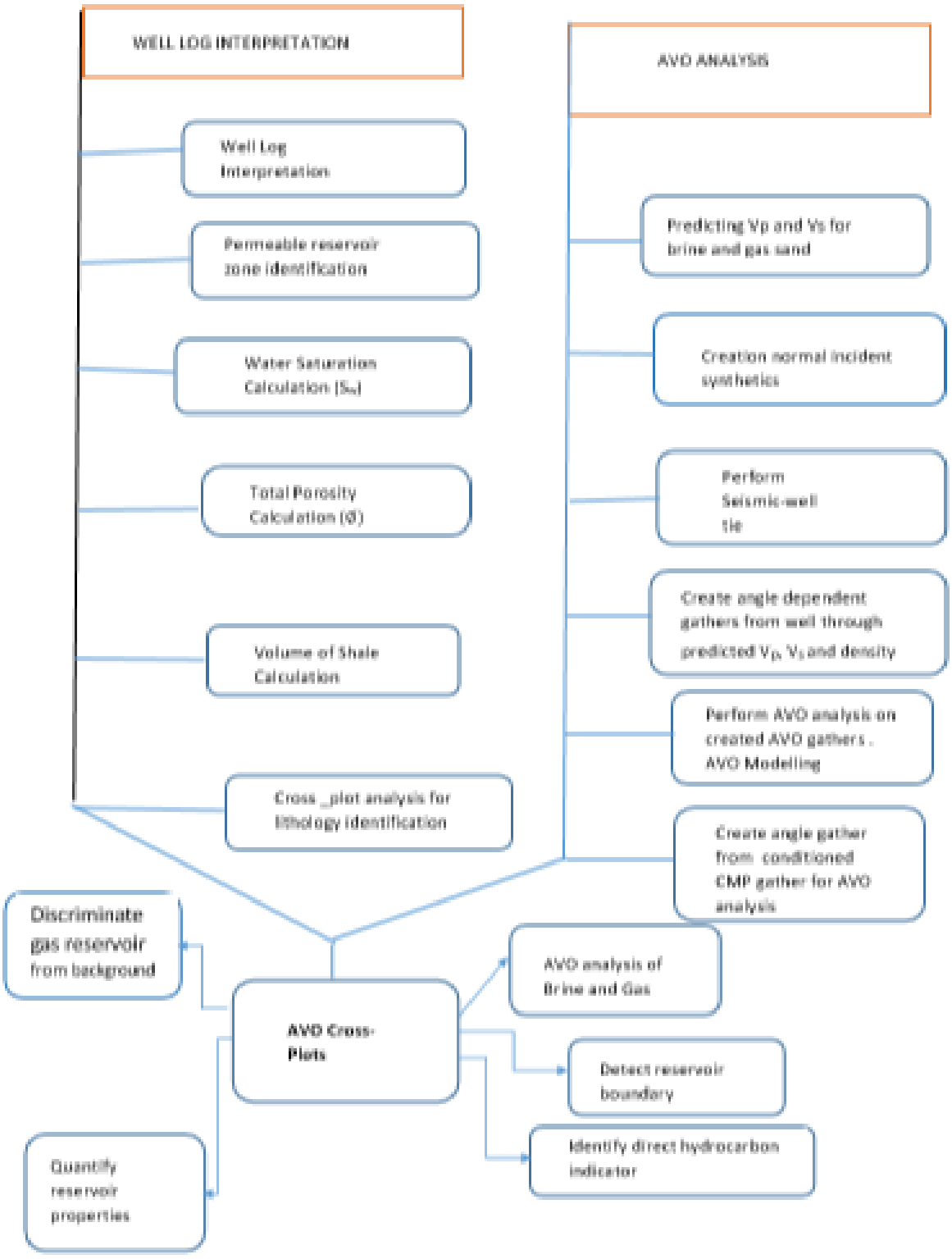

FIG. 8. Work flow for the Research.

Methods

The techniques adopted in this research were correcting well logs units parameters and to model the cross-plot of well-log, the use of petrophysics equations ,AVO attributes to generate rock physics parameters such as Lamda-rho, mu-rho and poison impedance whose rock characteristics can be extracted from well logs data. The cross-plot was analysed to estimate fluid with lithologies properties. Having successfully imported the log data , we edited the log and also conditioned it for better interpretation. Checkshot correction and median filtering was done to edit the logs.

Analysis Of The Data For Avo Studies Using RokDoc Software

The use of RokDoc software was employed to perform Gassman fluid substitution. Pre-stack seismic gather for far, near and full offset were generated. The essence of the binary header and trace header display was to tie the data information with the software for its smooth running. The near, far and full seismic gathers plots shows the behavior of the wiggles express in phase (Figure 8). The wiggles are displayed in red for the near , far and full offset while the well logs excursion shown is black colour.

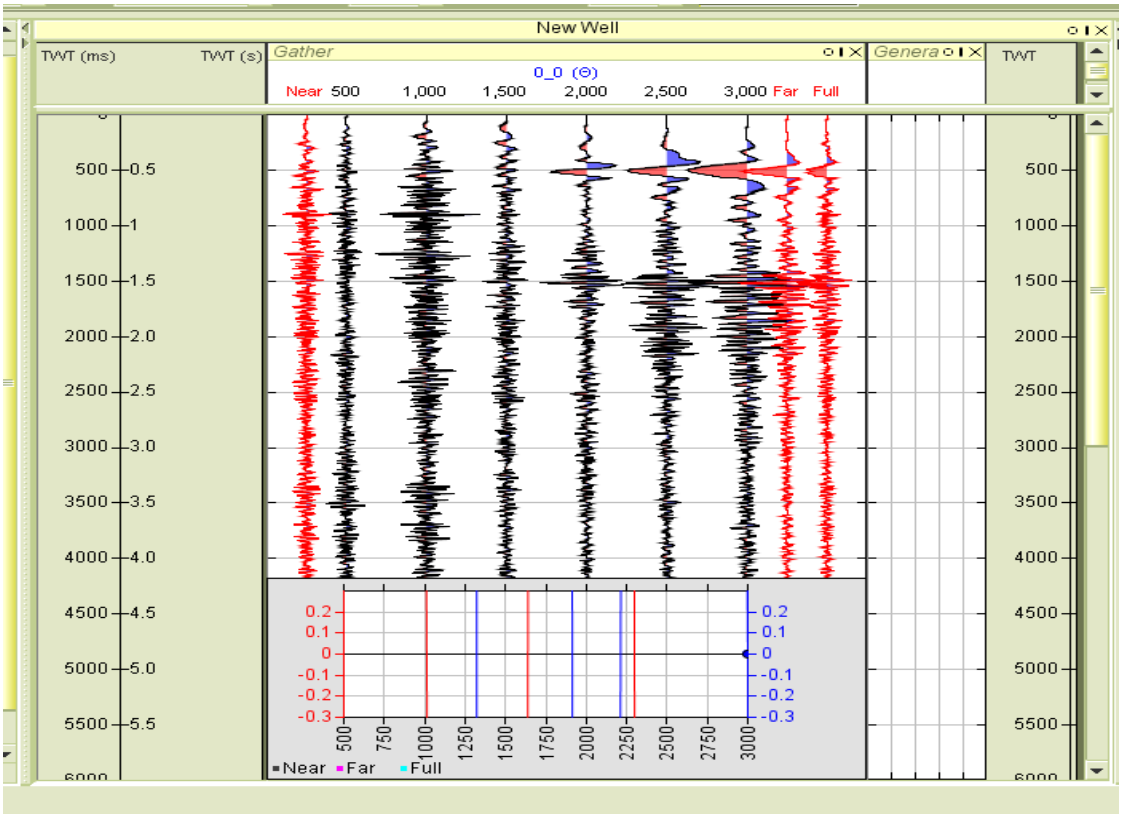

FIG. 8:Super Seismic Gather for Near, Far and full stacks

Algorithms Employed For Data Analysis

During data analysis the following equations were used

$$R(\theta) = R(0) + \left[\frac{9}{4}(\sigma_2 - \sigma_1) - R(0)\right] Sin^2\theta \quad (1.)$$

$$= R(0) + GSin^2\theta \quad (2.)$$

Where R is the reflection coefficient for angle of incidence $\theta = 0$ (normal incidence) called the intercept I or amplitude G.

$$R_P = \frac{1}{2}\left[\frac{\Delta V_P}{V_P} + \frac{1}{4}\frac{\Delta V_P}{V_P}\right] = \frac{5}{8}\frac{\Delta V_P}{V_P} \quad (3.)$$

$$\frac{\Delta V_P}{V_P} = \frac{8}{5}R_P \quad (4.)$$

$$\frac{\Delta V_S}{V_S} = 2R_S - \frac{1}{4}\frac{\Delta V_P}{V_P} = 2R_S - \frac{2}{5}R_P \quad (5.)$$

$$= (R_P - G) - \frac{2}{5}R_P = \frac{3}{5}R_P - G \quad (6.)$$

Thus , ${}^{\Delta V_P}/_{V_P}$ and ${}^{\Delta V_S}/_{V_S}$ simplified using linearly combining R_p and G.

Now " Fluid factor" F:

$\Delta F = \frac{\Delta V_P}{V_P} - 0.58\frac{\Delta V_S}{V_S}$(assuming$\frac{V_P}{V_S} = \frac{1}{2}$)

$$= \frac{8}{5}R_P - 0.58\left[\frac{3}{5}R_P - G\right] \quad (7.)$$

ΔF

$$= 1.252R_P + 0.58G \quad (8.)$$

AVO Attributes Calculation

In calculating intercept $*$ gradient (I$*$ G) attributes the approach to used involves multiplying two fundamental AVO attributes . It was presented as '' product stack displays''.

This can be inspected to ascertain the behavior . Fluid factor (FF) attribute was estimated. The FF attributes was proposed as:

I-G cross-plot technique

The attributes was performed using linearized stack which places I and G in a range of values. The values when cross-plotted arrives at new (l-G) plots, their contrast also called wet-rock line was estimated. This wet-rock line likened to lithologic trend or mudrock line used by authorities. Their separations based on data points depicts wet-rock line of fluid – factor . This wet-rock line displayed assumed to follow a median regression line gotten from the cluster data points as opined by Foster et al.,(1993),;Ross (2000) ; Veeken et al.,(2002).

The plots interpreted as gas-filled – reservoir data points plotted scattered more away from the regression line. This display have forms named butterfly shape: those plots which trends along the central-line with clouded points in two regions placed in a symmetrical manner.

(b,) Vp-Vs cross-plot technique

This plots of mudrock lines establishing the residual error is a least square technique which measures fluid factor (Smith & Gidlow , 1987; Smith & Sutherland, 1996).

$$FF = -\frac{29}{25} R_P \left({}^{V_P}/_{V_S}\right) R_S \qquad (9.)$$

R_P is the compressional wave reflection coefficient and R_S is the shear-wave reflection coefficient . We can also employ a specific gradient using mudrock line, as envisaged by Castagna et al.,(1985).

$$V_P = 1.16 V_S + 1360\ m/s \qquad (10.)$$

According to Aki et al,(2002) , they restructured the Zoeppritz algorithm using approximation method as:

$$R(\theta) = a\frac{\Delta V_P}{V_P} + b\frac{\Delta \rho}{\rho} + c\frac{\Delta V_S}{V_S} \qquad (11.)$$

Where $a = \frac{1}{(2Cos^2\theta)} = \left(\frac{1+ tan^2\theta}{2}\right)$, $b = 0.5 - \left[\left(\frac{2V_{S^2}}{V_{P^2}}\right) Sin^2\theta\right]$, $c = -\left[\frac{4V_{s^2}}{V_{P^2}} Sin^2\theta\right]$

$$V_P = \frac{\left(V_{P1} + V_{p2}\right)}{2} \ ; \ V_s = {}^{(V_{S1} + V_{S2})}/_{2} \ , \rho = \left(\frac{\rho_1 + \rho_2}{2}\right)$$

$$\Delta V_P = V_{P2} - V_{P1} \ ; \ \Delta V_s = V_{S2} - V_{S1} ; \ \Delta \rho = \rho_2 - \rho_1 \ ; \ \theta = \frac{\theta_i + \theta_t}{2} ,$$

Where $\theta_t = \arcsin\left[\left(\frac{V_P}{V_S}\right) Sin\theta_i\right]$

Also , Smith and Gidlow (1987) again approximated Aki and Richards algorithm as:

$$R(\theta) = \frac{1}{2}\left(\frac{\Delta V_P}{V_P} + \frac{\Delta\rho}{\rho}\right) - 2\frac{V_P^2}{V_S^2}\left(2\frac{\Delta V_P}{V_P} + \frac{\Delta\rho}{\rho}\right) Sin^2\theta + \frac{1}{2}\frac{\Delta V_S}{V_S} tan^2\theta \qquad (12.)$$

Next , Equation 11 was simplified, here the density aspect was removed by applying Gardner et al.,(1974), we get:

$$\rho = aV^{\frac{1}{4}} \qquad (13.)$$

Whereby when differentiated we arrived:

$$\frac{\Delta\rho}{\rho} = \frac{1}{4}\frac{\Delta V_S}{V_S} \qquad (14.)$$

Substituting equation (14) solve using least squares technique for deriving weights interpreted into seismic event producing estimation of attributes

$\Delta V_P/_{V_P}$ and $\Delta V_S/_{V_S}$.

Further derivation was done by Smith & Gidlow (1987) to give two more stacks called '' Pseudo-Poisson's ratio reflection coefficient, defined as:

$$\frac{\Delta\sigma}{\sigma} = \frac{\Delta V_P}{V_P} - \frac{\Delta V_S}{V_S} \qquad (15.)$$

and the event also known as fluid factor stack. In deriving the fluid- factor , Smith & Gidlow (1987) applied ARCO mudrock algorithm named a straight line fits appeared valid for water saturated clastics of the whole world. This algorithm can be written thus

The equation is written as :

$V_P = 1360.0 + \frac{29}{25} V_S$(velocities in m/s) (16.)

Equation (25) when differentiated gives :

$$\Delta V_P = \frac{29}{25}\Delta V_S \qquad (17.)$$

Expressing equation (17.) in ratio form gives :

$$\frac{\Delta V_P}{V_P} = 1.16\frac{V_S}{V_P}\frac{\Delta V_S}{V_S} \qquad (18.)$$

According to Smith & Gidlow (1987), they noticed that equation (18.) is valid for wet scenario. For an hydrocarbon rich porous formation equation (18) is not valid the fluid factor is given as :

$$\Delta F = \frac{\Delta V_P}{V_P} - 1.16\frac{V_S}{V_P}\frac{\Delta V_S}{V_S} \quad (19.)$$

Based on our research , algorithm (16) was refined as:

$$V_P = 1550 + 0.807V_S \quad (20.)$$

When Zoeppritz equation is approximated ,we get:

$$R(\theta) = R_P + GSin^2\theta$$

Where R_P = P-wave intercept , G = gradient

$$R_p = \frac{1}{2}\left[\frac{\Delta V_P}{V_P} + \frac{\Delta\rho}{\rho}\right]$$

$$G = R_p - 2R_S$$

$$R_S = \frac{1}{2}\left[\frac{\Delta V_S}{V_S} + \frac{\Delta\rho}{\rho}\right]$$

$$R_P = G + 2R_S$$

$$G = \frac{1}{2}\left[\frac{\Delta V_P}{V_P} + \frac{\Delta\rho}{\rho}\right] - 2\left[\frac{1}{2}\frac{\Delta V_S}{V_S} + \frac{\Delta\rho}{\rho}\right]$$

$$\frac{8}{5}R_P = \frac{\Delta V_P}{V_P}$$

In the Smith and Gidlow (1987) approximations , the actual physical parameters $\Delta V_P/V_P$ was determined.

Therefore, from Gardner et al.,(1974) the formula named (13) ,two approaches equates each other.

Method 1, replaced formula (23) to relates R_P to arrived at:

$$R_P = \frac{1}{2}\left[\frac{\Delta V_P}{V_P} + \frac{1}{4}\frac{\Delta V_P}{V_P}\right] = \frac{5}{8}\frac{\Delta V_P}{V_P} \quad (21.)$$

Giving rise to :

$$\frac{\Delta V_P}{V_P} = \frac{8}{5}R_P \quad (22.)$$

Replacing formula (23) in the relation, R_S , gives

$$R_S = 0.5\left[\frac{\Delta V_S}{V_S} + 0.25\frac{\Delta V_P}{V_P}\right] \quad (23.)$$

Or :

$$\frac{\Delta V_S}{V_S} = 2R_S - \frac{1}{4}\frac{\Delta V_P}{V_P} = 2R_S - \frac{2}{5}R_P$$

$$= (R_P - G) - \frac{2}{5}R_P = \frac{3}{5}R_P - G \qquad (24.)$$

Thus , ${\Delta V_P}/{V_P}$ and ${\Delta V_S}/{V_S}$ simplified using linearly combining Rp and G.

Also from Pseudo –Poisson's ratio reflection coefficient the formula (15.) becomes :

$$\frac{\Delta\sigma}{\sigma} = \frac{\Delta V_P}{V_P} - \frac{\Delta V_S}{V_S}$$

$$= \frac{8}{5}R_P - \left[\frac{3}{5}R_P - G\right]$$

$$\frac{\Delta\sigma}{\sigma} = R_P + G \qquad (25.)$$

Now " Fluid factor" F:

$\Delta F = \frac{\Delta V_P}{V_P} - 0.58\frac{\Delta V_S}{V_S}$(assuming$\frac{V_P}{V_S} = \frac{1}{2}$)

$$= \frac{8}{5}R_P - 0.58\left[\frac{3}{5}R_P - G\right]$$

$$\Delta F = 1.252R_P + 0.58G \qquad (26)$$

Fatti et al., (1994) formulated an equation to solve for P- and S- reflectivities thus :

$$R(\theta) = \frac{1}{2}\left(\frac{\Delta I_P}{I_P}\right)(1 + tan^2\theta) - 4(\frac{V_S}{V_P})^2\left(\frac{\Delta I_S}{I_S}\right)Sin^2\theta \qquad (27.)$$

This equation is tested to be useful for angle < 50 degrees.

Well – Log Rock Attribute Estimation

Rock physics algorithm generated using Hampson Russell eLOG and RokDoc tool. Estimation of rock attribute were generated using input log data . The attributes estimated were S-wave velocity from Castagna's algorithm (equation 10). The polynomial fitting of order two were employed

$$V_s = aV_p{}^2 + bV_p + C \qquad (28.)$$

For sand and shale lithology , Latimer (2004) gave a formula thus:

$$V_s = 0.862V_p - 1.172 \qquad (29.)$$

The relation above (equation 10) is depends on the rock unit . For purpose of precision.

Sandstone,

Sands $V_s = +\frac{201}{250}V_p + \frac{107}{125}$ (30.)

Limestone $V_s = -\frac{11}{200}V^2 + 1.017V_p - \frac{206}{200}$

Dolomite $V_s = +0.583V_p - 0.078$ (31.)

Shale $V_s = +0.770V_p - 0.867$ (32.)

Incident Angle And Offsets Distance Extraction

The synthetics was produced by employing Hampson Russell software for various offset. In each case , the incident angle generated for all the events (gathers) , offsets(receivers-source distance), time also named depth were sampled .Based on velocity model, the source - receiver location , the angles of incidence employs ray tracing technique were determine .

The next steps adopted were picking all the amplitudes for all offsets in each time intervals. Since amplitudes remains a very useful tool in seismic analysis, it good and proper management must be adhered to for good reservoir characterization.

Amplitudes are highly useful in seismic inversion work, to analyze amplitude with respect to angle of incidence , conversion of each offset to its angle of incidence can be achieved using ray tracing approach. According to Veeken (2007) , the data shape cloud seen within I and G cross-plot gives a clue to phase rotation of the data.

It shows the plots of various phase rotation suggested as muted CMP gathers for (30^0 increment). The data spread suggests degree of rotation. The largest symmetry indicates the direction of phase rotation.

Conditioning Of Well Logs

Well logs data which were gamma ray, caliper, resistivity , sonic (P-waves), density , Neutron-porosity and self-potential (SP) were all present in well 02 which motivated the choice of this well for this study. Throughout the vertical zones chosen for this study the quality of the well log

data were good. Checkshot data were also present in well 02 enabling tying seismic data to well log data to generate synthetics. (Figure 17). Well markers (designated top and bottom) were also employed for the study. All the well logs data chosen for this study were well-02 , 06 and 07 were properly conditioned/ edited before they were used for modeling workflow. Various steps of analysis done on the data were :

Filtering to De-spiking for removal and/or correction of irrelevant data point.

Linearized logs to correct range and remove irrelevant porosity , clay content, water resistivity and saturation .

Computation of volumetric curves $\emptyset_{total}$, volume of clay and water saturation.

Correction of density logs and sonic logs of mud filtrate invasion.

Volume of shale computation.

Validation ,depth matching and environmental condition of acquisition of logs data were considered. Splicing of logs with multiple run was done.

Determination Of Porosity

It has been known and accepted generally by geologists that when calculating porosity it is more accurate to used bulk density. To compute the pore spaces (porosity), density of roc\k matrix ' ρ_{ma}', fluid density ,'ρ_F' the bulk density 'ρ_b'. The overall average density of sandstone equals 2.68 g/cm3, that of shales as 2.67g/cm3.If the well encountered hydrocarbons or water this affect the fluid density. From the electrical resistivity logs , the density can be computed using constituent and phase behavior, $\rho_{oil} = 0.8g/cm^3, \rho_{gas} = 0.6\ g/cm^3$.

Assumption here is that $\rho_{water} = 1$. Considering gamma ray value to be threshold value in this case 100GAPI is noted , the rock unit delineated as sandstone.

$$\varphi_{density} = \frac{\rho_{ma-\rho_b}}{\rho_{ma} - \rho_f} \qquad (33.)$$

Where ρ_{ma}= matrix (or grain) density ,ρ_f = fluid density and ρ_b= bulk density (as measured by the tool and hence includes porosity and grain density).

Transit Time Estimation Using Sonic Log

From sonic log, interval transit time relates in direct proportion to acoustic velocity which depends on rock units term formation and spore spaces called porosity. The sonic log records the time taken for acoustic (sound) wave to travel one-foot of a formation.

The sonic log velocities were crossed-checked with TWT (two-way travel time), seismic velocity (checkshot) data.

The time term transit time (interval) sampled at regular depth interval . The acoustic velocities were obtained and estimated taking the reciprocal of the interval transit time Δt.

$$V_P = \frac{1}{\Delta t}(ft[\mu s]^{-1}) \quad (34.)$$

Poisson's ratio ,σ , is defined as:

$$\sigma = \frac{0.5(\frac{V_P}{V_S})^2 - 1}{(\frac{V_P}{V_S})^2 - 1} \quad (35.)$$

Determination Of Shear And Compressional Acoustic Impedances

The wave propagated usually is affected by the medium of its propagation known as seismic impedance I defined as the product of seismic wave velocity (v) and density (ρ) of the rock (I=ρV) . When seismic wave propagates across the interface of two contrasting rocks characterized by different impedance , part of the pulse will be reflected , while others are transmitted via the contrasting interface. The magnitude of the maximum upward displacement (amplitude) named reflectivity coefficient, R ,rely on the impedance difference existing between the two boundaries causing the waves.

$$R = \frac{I_2 - I_1}{I_2 + I_2} \quad (36.)$$

Where $I_i = \rho v$. Based on available seismic work, the time taken for a reflected wave to arrived at the receiver from a boundary . We can determine shear impedance $I_S$as:

$I_s = V_S \rho \, X \, 10^2$ (g/cm-3)

Where V_S measured in m/s and ρ is in g/cm3.

P- wave acoustic impedance ,I_P given as :

$$I_P = V_P \rho \, X \, 10^2 (g/cm^2 s) \quad (37.)$$

Where V_p is measured in m/s, ρ in g/cm3.

Algorithm For Bulk And Shear Moduli Of Elastic Material

Based on algorithm shear wave velocity relates to shear moduli as:

$$\mu = {V_S}^2 \rho \; X \; 10^{-5} (MPa) \qquad (38.)$$

Whereμ stands for shear modulus, V_S stands for shear wave velocity . Also the shear modulus relates to bulk modulus as:

$$K = \left[{V_P}^2 \rho - \frac{4\mu}{3} \right] X \; 10^{-5} (MPa) \qquad (39.)$$

Estimation Of Permeability (K)

Formation volume factor generated for shally sands as :

$$F = \frac{1.65}{\varphi^{1.33}} \qquad (40.)$$

Where φ is porosity.

Permeability (K) links to Formation Factor

$$K = \frac{(7.0 \; x \; 10^8)}{F^{4.5}} \qquad (41.)$$

Estimation Of Sw (Water Saturation)

The calculation of Sw (water saturation) was done for the virgin zone (uninvaded section) of the borehole. Here water resistivity , Rw, at a particular temperature of the formation was needed. It was computed using porosity and resistivity logs around a clean water section. We employ Archie method named inverse approach as:

$$R_w = \frac{\varphi^m \; x \; R_t}{a} \qquad (42.)$$

Where R_w stands for water resistivity at formation temperature ,φ stands for porosity , R_t stands for deep resistivity , a stands for tortuosity factor, and m represents cementation factor , when

m=2 , it depicts sands. In water saturated zone Sw=1 . Also Rw stands for water resistivity at a specific temperature denoted as Rwa , m=1.50 , a= 2.0 and Rt can be read from the log.

The formula named '' Archie algorithm'' shows how water saturation is related to formation resistivity thus:

$$S_w{}^n = \frac{F.R_w}{R_t} \qquad (43.)$$

Where S_w = water saturation ; n = saturation exponent =2 ;

$$S_w = \sqrt{\frac{F.R_W}{R_t}} \qquad (44.)$$

Substituting for F from Equation (22) , Equation (26) becomes :

$$S_W = \sqrt{\frac{1.65\ x\ R_w}{\varphi^{1.33}\ x\ R_t}} \qquad (45.)$$

RESULTS AND DISCUSSIONS

Far, near and mid offset

From the velocity data generated reflectivity data. This was plotted against square of the sine of the angle of incidence for near and far reflections. The plot of offset distance versus angle of incidence (in degree), the far offset corresponds to larger angle of incidence > 30 ^{0}which ranges between 5000 m and above ,the near offset between 0 to 1000 m corresponds to angle of 10^0 and below. Also the plot of TWT (ms) versus offset distance (Figure 9a and 9 b).This shows a clear cut distinction between near, far and full offset.

The actual depth at which the p-wave velocity was acquired was noted to tie the synthetic and seismic event. This assisted in extrapolating the actual Vp values. The check shot correction (Figure 10) which changes the depth versus time plot links the sonic log to enhance tying the synthetic and real seismic data . The significant of this is

to extrapolate compressional wave velocity (V_P) to the surface often overestimated near the surface. The left hand of the diagram show sonic curves , the original curve in red and correction effect displayed in black.

Fundamentally, rock physics relates components such as velocity- porosity, impedances, lame's parameters and V_P/V_S used in interpreting lithofacies. AVO attributes and inversion were used to compute litho-fluid parameters. Basic rock physics relation such as velocity – porosity, impedances, Lame's parameters and V_p/V_s among others were defined for the lithofacies. This was followed by computations of the litho-fluid dependent seismic attributes of interest for AVO analysis and inversion.

The essence of the binary header and trace header display was to tie the data information with the software for its smooth running. The near, far and full seismic gathers plot shows the behavior of the wiggles express in phase. The wiggles are displayed in red for the near, far and full offset while the well logs excursion shown in black colour.

Interpretation of AVO attributes

From the prestack time migration display the seismic section here shows a bright and flat spot which were areas of pronounce amplitude , penetrated by well-02. This were confirmed in the crossplot of I$*$ G attribute interpreted as gas shows. From the crossplot amplitude versus $Sin^2\theta$ this zone falls within the mid offset , confirmed using the wet rock trend falling within sandstone/shale bottom gas reservoir (Figure 11). The fluid factor attribute indicated the region were riched of gas reservoir.

Synthetic generation at various offset angles were carried out, in each case the angle of incidence for all the gathers , offset and depth(time) samples generated. At every point given the source- receiver located here the incident angle which employs ray tracing approach was done. Followed by picking all amplitudes information (from

specific common mid point event/gather) of all source – receivers distance (offset) per time sampled intervals.

In the seismic data, migration was done named pre-stack depth migration for AVO analysis , collapsing the diffractions at targeted depth smaller compared to fresnel zone thus increasing lateral resolution. Amplitude preserved during pre-stack depth migrated (PSDM) exercise done. Finite difference technique used in pre-stack migrations employed, increases stratigraphic resolution , data quality and accurate location.

From figure 12 above , the gamma ray log between the interval of 7620 -7850ft depict sand formation due to it low gamma ray values , resistivity log value is high indicating hydrocarbon rich formation. Again the interval of 7650-7720 ft the formation is characterized by high gamma ray values indicating the delineation shaley formation , resistivity value is low indicating shale formation. Between 7730-7760 ft the formation has a high resistivity value suggesting hydrocarbon and low gamma ray value showing gas sand bearing formation.

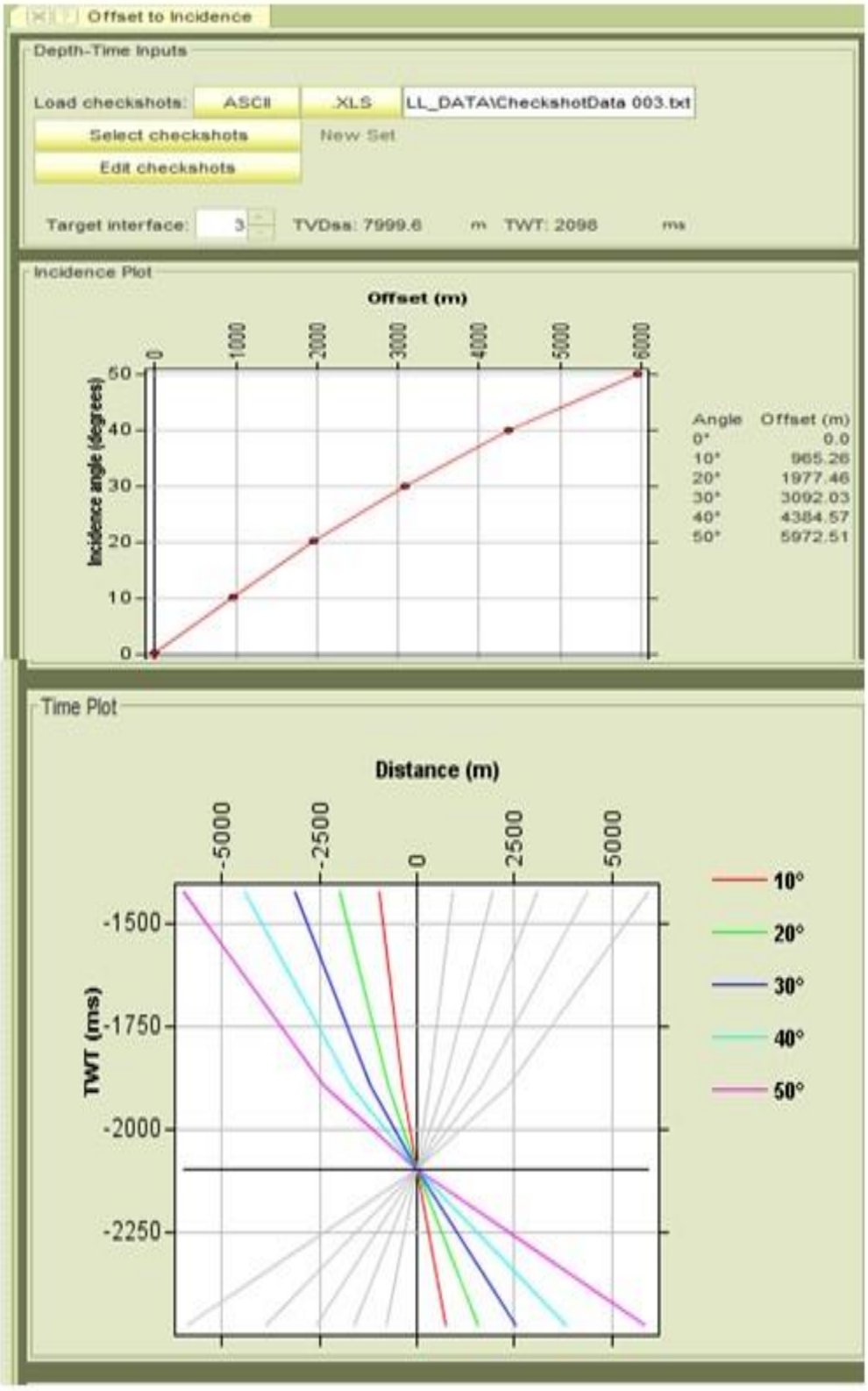

FIG. 9 (a.) : Plots of Offset distance against Incidence Angle
9 (b.) : Plots of Offset distance against TWT

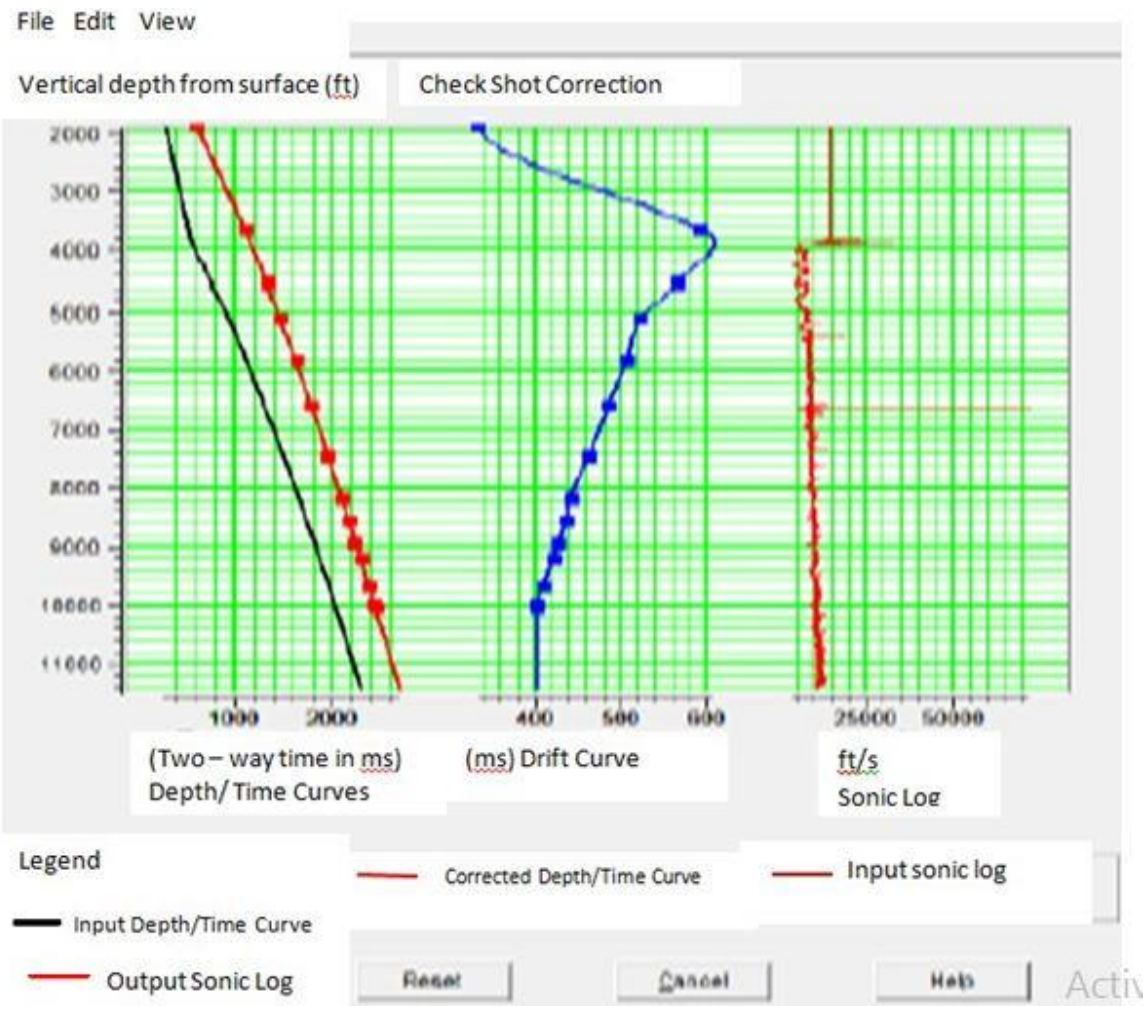

FIG.10: Check shot correction applied to sonic log data.

.

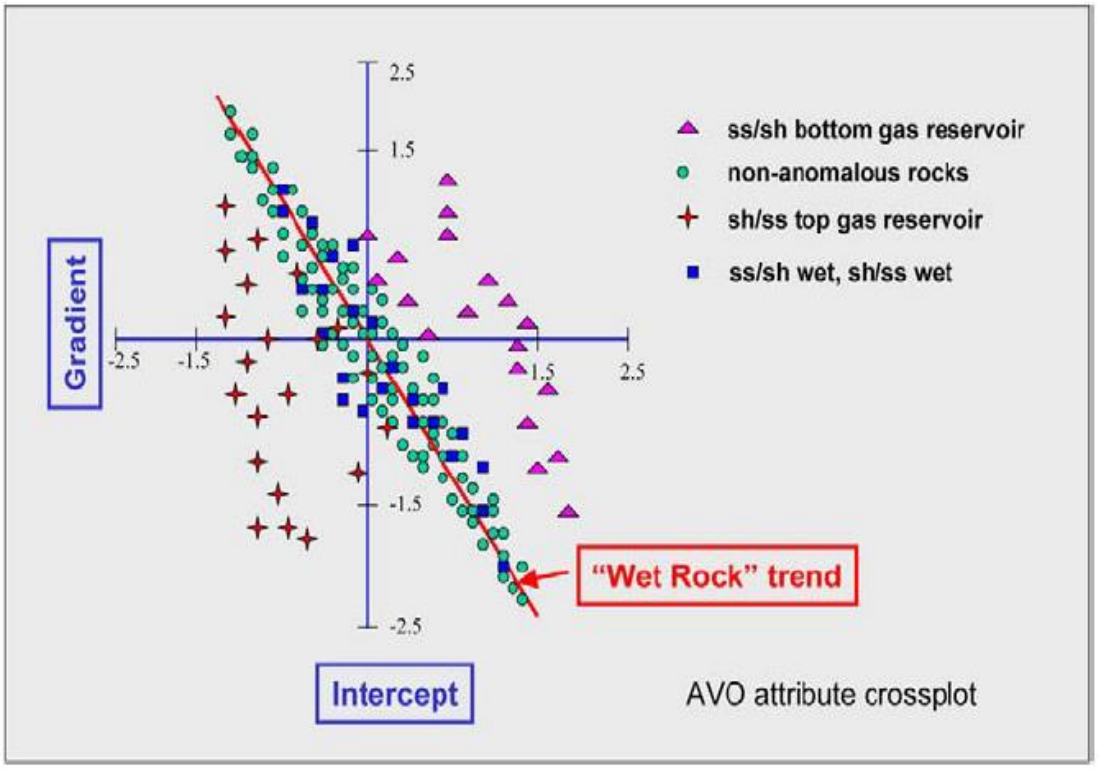

FIG 11 : Cross-plot of intercept (l) versus gradient (G). By multiplying a factor brings two attributes closer in line with each other named weighted axis. The regression line termed ‘wet-rock ‘, the distance to this line estimates the fluid factor magnitude. The configuration of points (cloud) depicts a butterfly shape (clouds points of positive and negative values away from the main trend) shown only when hydrocarbon are suspected

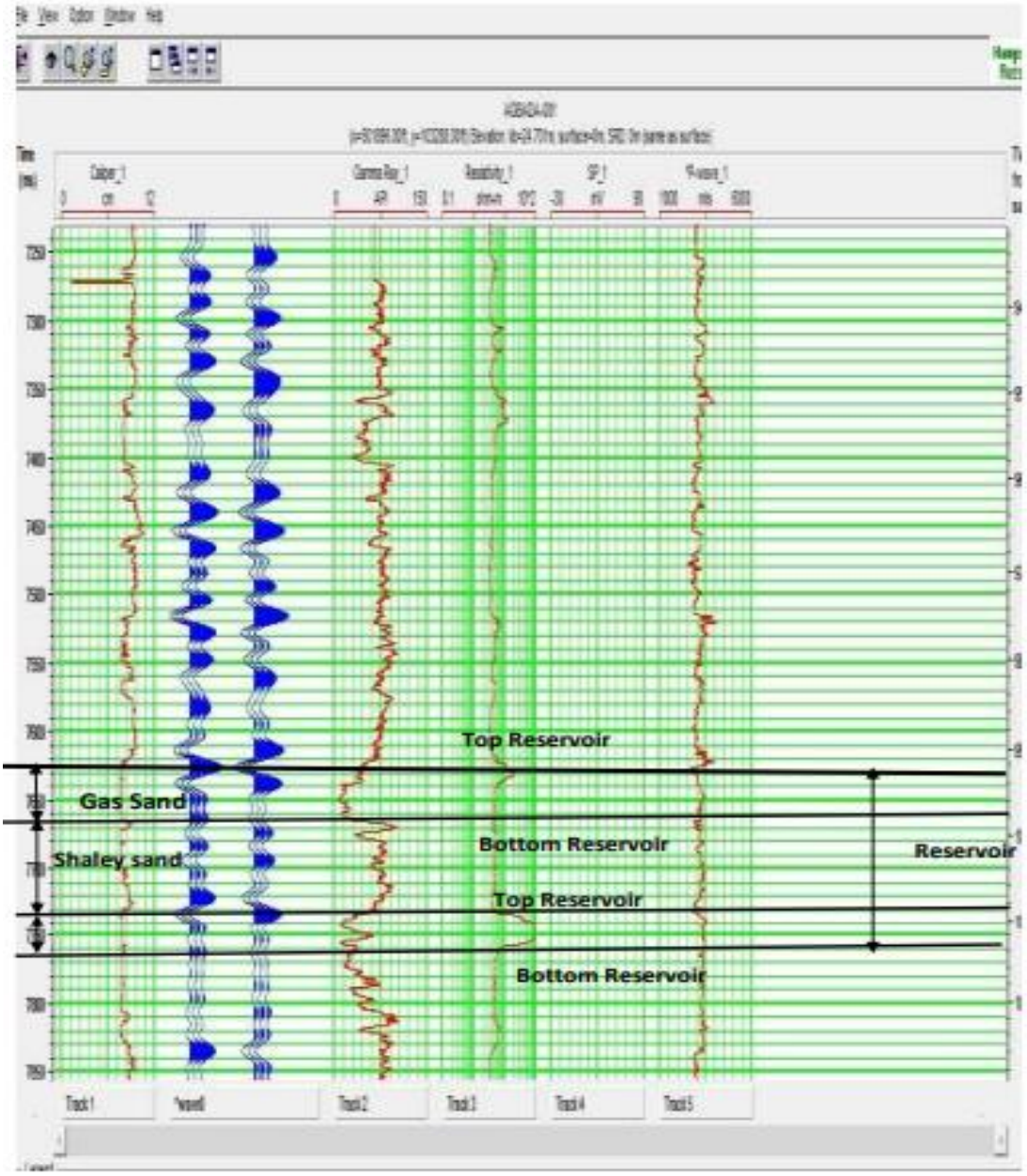

FIG 12: Well AGB 1 indicate caliper, gamma ray, resistivity, SP and sonic logs interpreted for rock unit, mineralogical content (volume) and delineated horizon

Prestack inversion

After inverting the prestack Seismic data, evidences of direct hydrocarbon indicators like bright spot was evidenced and this give a clue on the presence of hydrocarbon in the area. This is shown in figure 13.

The crossplot of inverted -V_pV_s versus offset (in ft) display a section indicating bright spot. This section gives clue of presence of hydrocarbon as shown within the yellow eclipse in Figure 13.

Also, the inversion of acoustic impedance cross-plotted with offset (in ft) further strengthen this evidence in confirmation.

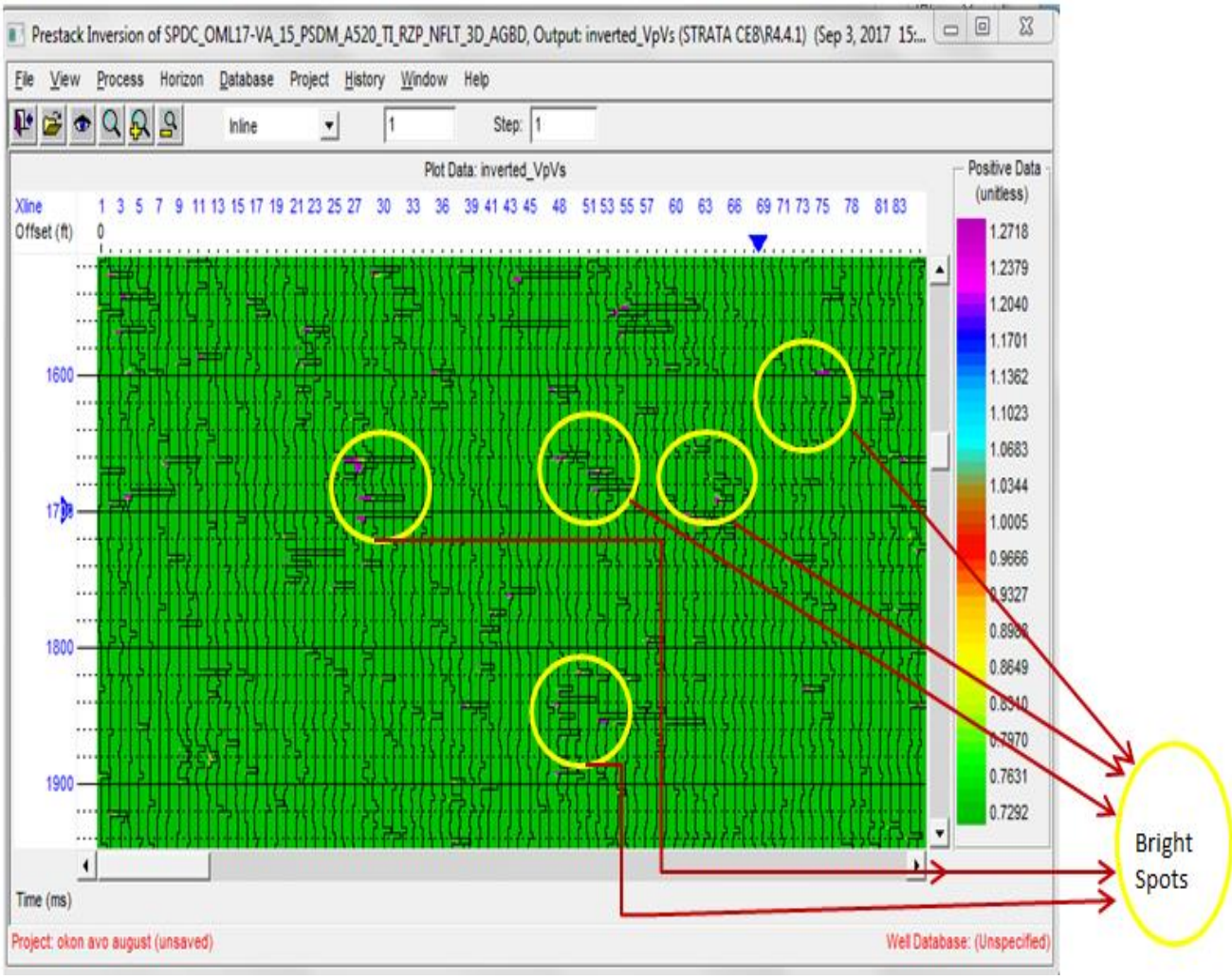

FIG 13: The inverted seismic data showing bright spot as direct hydrocarbon Indicator.

Amplitude Versus Offset (AVO)

The synthetics generated during AVO, the depth was calibrated in time selected as shale saturated with gas sand boundary, shale saturated with oil sand boundary, shale saturated with brine sand boundary and amplitudes at different offsets, synthetic extraction was done. The depths selected corresponds to TWTs of 2100 and 2200 ms, the point at which heterogeneous begins. To identify hydrocarbon or brine boundary synthetics can be employed using fluid curves. On extracting the amplitudes (Table 2), amplitudes were cross-plotted versus incidents angles (Figure 14 and 15). This brought out the link between hydrocarbon/brine with anomalous amplitude noticed in synthetic (seismograms).

Castagna (1985) showed in similar reservoir, that the top reservoirs was identified according to the amplitude behavior whose link to offset on a common depth point (CDP) stack interpreted as hydrocarbon filled porous formation.

Class 1 possess higher reflectivity R_0 , amplitude positive with offset (called diming stack).

Class 2: Small positive R_0 changing from positive to negative amplitude versus offset (diming or brightening of reflection including polarity flip).

The brine sand here was characterized by water interpreted from the amplitude values of the data displayed.

-Class 3 shows negative $R_o$amplitudes getting more negative as offset increases (brightening of reflection) .

- Class 4 shows negative value of amplitude getting less negative as offset decreases (dimming reflection on gather/stack).

TABLE 2

Amplitude data at selected TWTs for well AGB 2

Time (ms)	Offset (Degree)	Amplitude	Fluid Type
2100	0	-0.00006	Hydrocarbon
	10	-0.00001	
	20	-0.00018	
	30	-0.00029	
	40	-0.0004	
2100	Offset (Degree)	Amplitude	
	0	-0.0002	Brine
	10	-0.00025	
	20	-0.00038	
	30	-0.00059	
	40	-0.0009	
2200	Offset (Degree)	Amplitude	
	0	-0.00061	Hydrocarbon
	10	-0.00615	
	20	-0.00625	
	30	-0.00637	
	40	-0.0065	
2200	Offset (Degree)	Amplitude	
	0	-0.001	Brine
	10	-0.0003	
	20	0.0006	
	30	0.002	
	40	0.004	

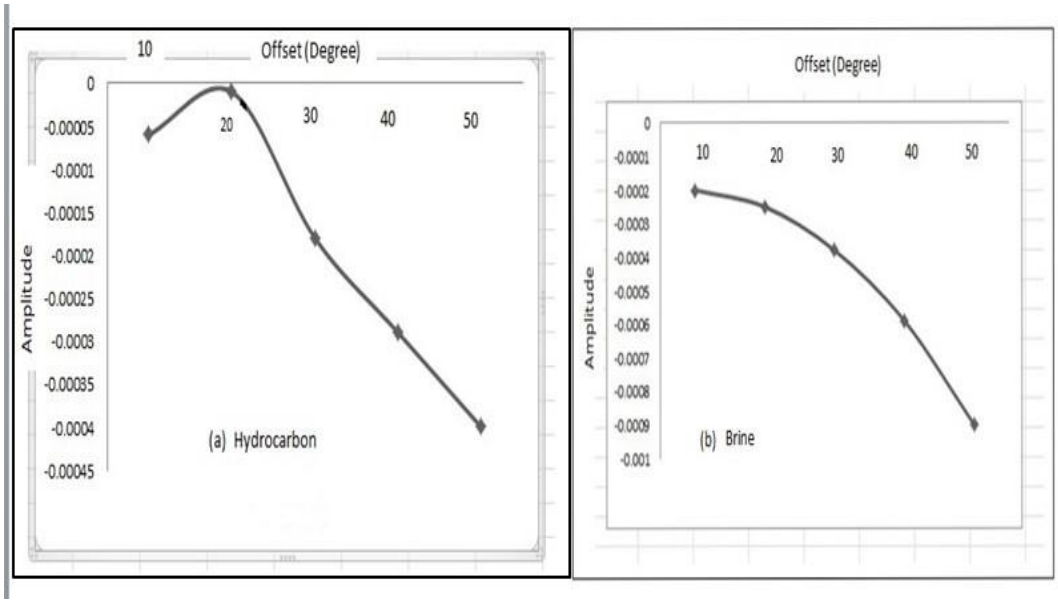

FIG 14. Amplitude versus angle crossplot at 2100 ms for AGB-2 (well)

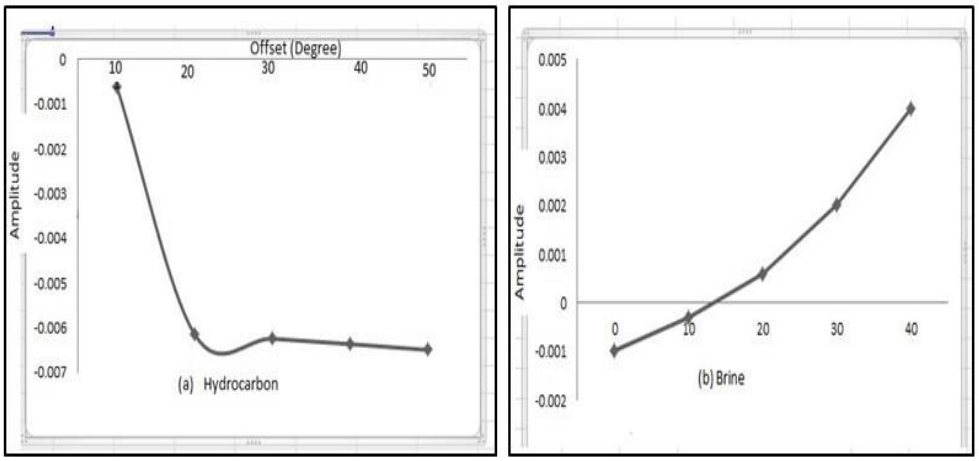

FIG.15 Amplitude versus angle crossplot at 2200 ms for AGB-2 (well)

AVO Gradient (G) , AVO Intercept ($\boldsymbol{R_P}$) And Fluid Factor ,($\Delta \boldsymbol{F}$)

Formulae 15,31,33 including 35, were used to estimate gradient/slope, (AVO), intercept and fluid factor. On a plot , observation shows that $\Delta F = 0$ depicted /interpreted as wet porous formations (reservoir). Result obtained showed that slope/gradient of amplitude versus offset, its intercept with inclusion of fluid factor were negative when linked (Figure 16,17,18 and 19). AVO outcome was linked to the located reflected wave based on the slope cross-plotted with intercept (Figure 16) , this falls in class l-gas sand, confirmed (Figure 16 and 17).

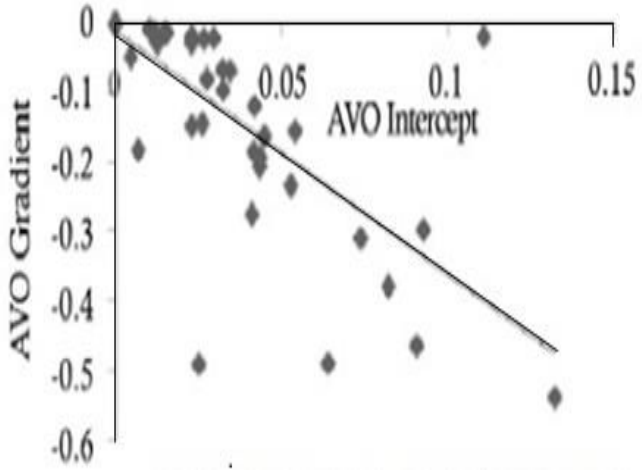

FIG 16 $\Delta\rho/\rho - R_P$ cross-plot.

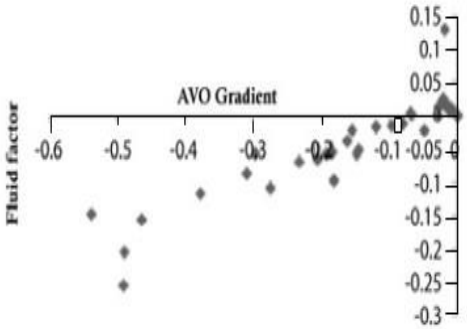

FIG.17 $R_S - R_P$cross –plot

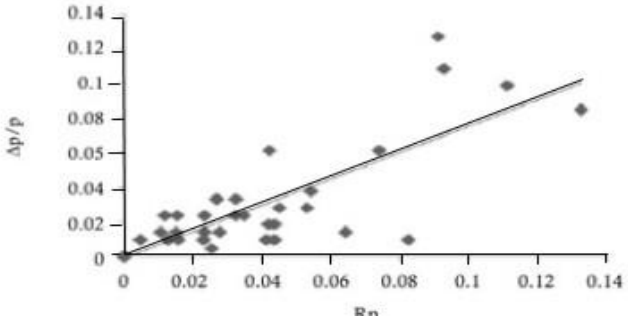

FIG. 18 Fluid factor – AVO gradient cross-plot.

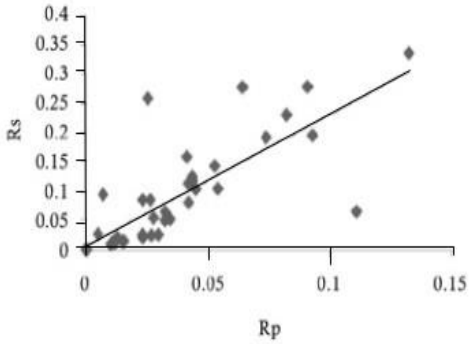

FIG.19 AVO Gradient–AVO Intercept Cross-plot

AVO Attributes

After careful analysis of the data, the result display on table 3 was generated for AVO attributes indicative of various rock types. This was used to characterized the reservoir .

Note: Kaver. = 0.34,Qaver.=0.57,Near stack angle = 300,Far stack angle = 450 .From the Dry model properties (KDry, mu, Rhodry, phi) . Kdry = 0.5, mu = 10, Rho dry = 1, Porosity = 0.25,Poisson's (Dry values) = -0.1, Kdry = 5 Gpa, Mu = 10 Gpa, Rho dry = 1 g/cm3, Vp= 4235m/s, Vs = 2886.6m/s, Rho = 1.2g/cm3.

The reflectivity was gotten by multiplying the density with the p-wave velocity also called reflection coefficient . The far and near offset was displayed when plotted the $Sin^2\theta$ against reflectivity . This indicated the behavior of material property of the various layers (Figure 20).

The far and near offset was display when we plotted the $Sin^2\theta$ against reflectivity. This indicated the behavior of material property of the various layers. This indicated the far and near offset proven as shown. Since anisotropy effects influences the AVO response .we used the polynomial fitting (linear) for correction of travel time in horizontal angle of a direction measured clockwise from north varies based on normal moveout impacts. AVO and horizontal angle of a direction measured clockwise from north results to linear fitting allowing for calculation of accurate AVO analysis . The essence was to ascertain the classes of AVO reservoirs outcome.

In plotting reflectivity versus $Sin^2\theta$ it reveals areas with complex AVO scenarios that was present at that time. (Figure19). This gave a pointer that anomalous pressure distributed may caused anisotropy within the reservoir. (Hilterman & Dunn,2004). Ascertaining the appropriate AVO analysis decision was done using figure 21. The plot of

Poisson ratio versus Acoustic Impedance (Figure 21) reveals the discrimination of gas and brine sand.The result displayed on table 4 reveals the reservoir parameters used for various cross-plot to ascertain the lithology evaluated for this study. The reflectivity was done by multiplying the density with the p- wave velocity also called reflection coefficient .

From the crossplot, poisson's ratio against acoustic impedance differentiated between brine gas and the gas sand (Figure 21). Evaluation and identification of the reservoir zone were done with the available data set, Petrophysical parameter for well-02 generated as shown on Table 4. The lithologic unit obtained by plotting the reflectivity ($V_p * Rho$) versus $Sin^2\theta$ for various mineral types/units.

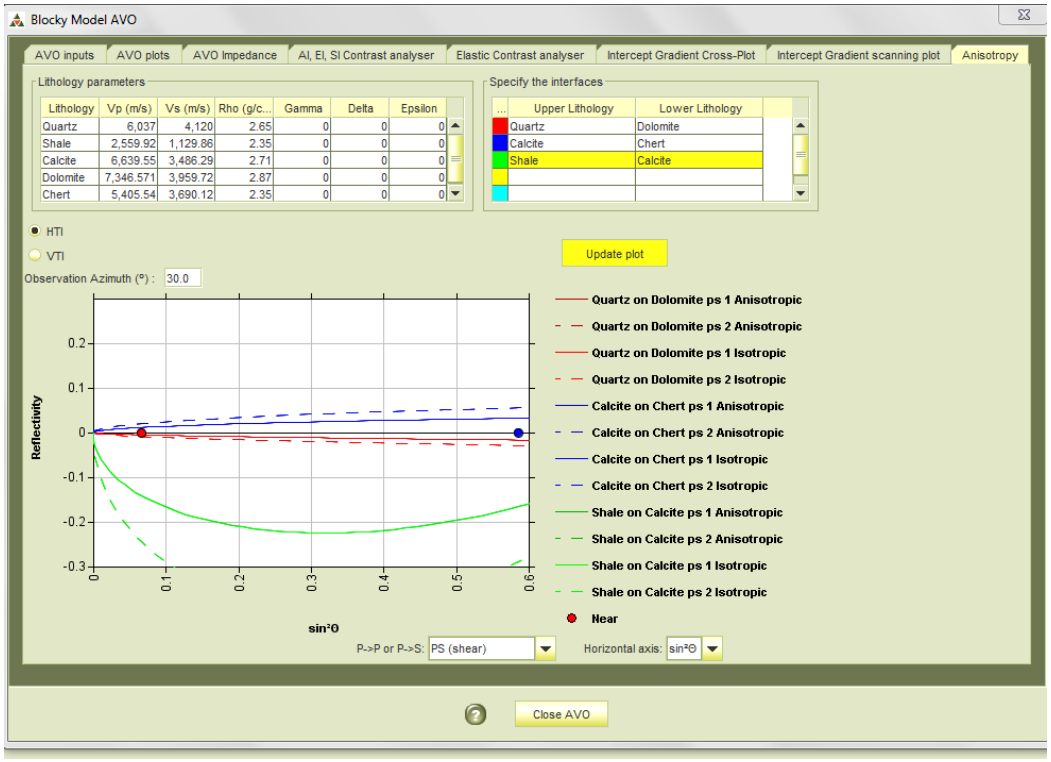

FIG.20: Shows Lithologic Parameters and the plot of Reflectivity versus Sin2θ

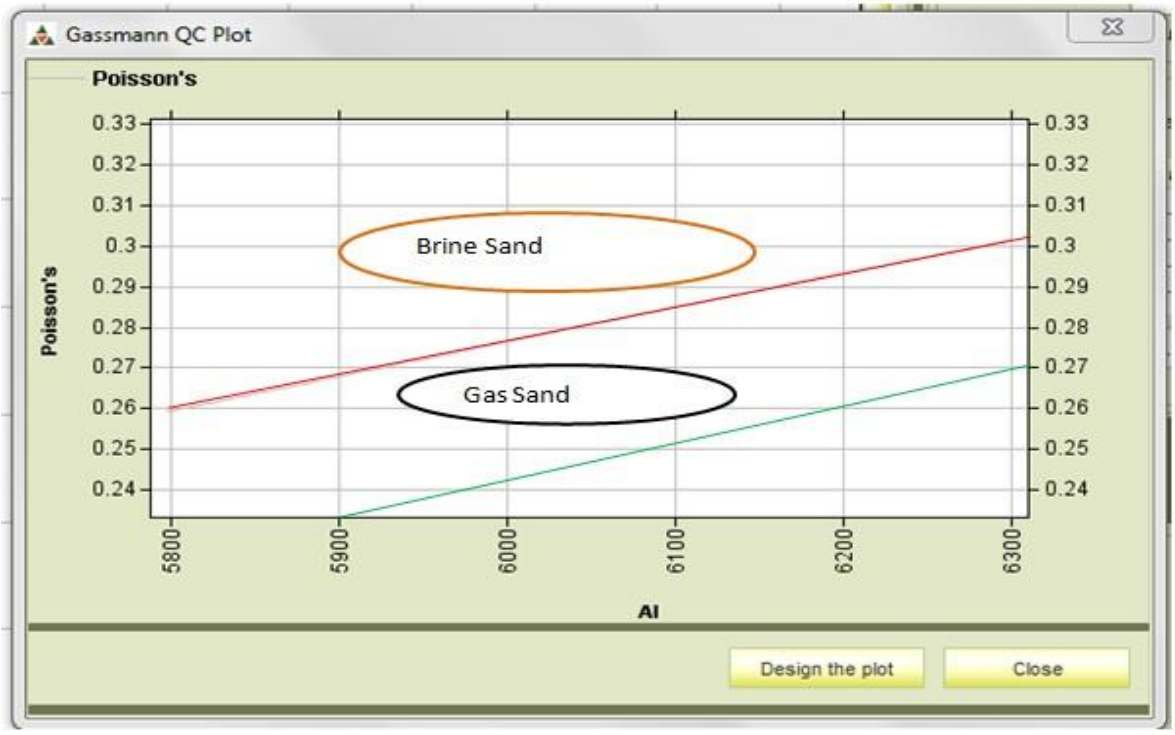

FIG.21 : Plot of Acoustic Impedance against Poisson's Ratio

TABLE 3
AVO attributes generated from the SPDC data

Units	Vp(m/s)	Vs(m/s)	Rho (g/cm^3)	K	Q	AI(g/cm)	SI	EI2	SEI2	K(Bulk)	PR(Poi.)	Lamda	E	Lamda	MuRho	Lamda
Quartz	6037	4120	2.65	0.466	0.683	15999.7	10920.2	352.6	37493	966	0.064	6.6	95.756	17.49	119.25	0.147
Shale	2559.92	1129.86	2.35	0.195	0.441	6015.8	2653.2	268.6	75242.11	15.4	0.379	9.4	8.274	22.09	7.05	3.133
Calcite	6639.55	3486.29	2.71	0.268	0.518	17993.2	9312.4	455.9	31219	119.467	0.317	55.467	84.293	150.315	86.72	1.733
Dolomite	7346.57	3959.72	2.87	0.291	0.539	21084.7	11364.4	488.0	39018	154.9	0.295	64.9	116.574	186.263	129.15	1.442
Chert	5405.54	3690.12	2.35	0.466	0.683	12703.0	8671.8	305.7	29071	68.667	0.064	4.667	68.073	10.967	75.2	0.146

Note: The AVO attributed generated for various units were made available by the Hampson Russel software.

The result of this display used for further characterization of the reservoir. (Source: SPDC)

TABLE 4

Estimated Petrophysical components for well -002

Well - 002	Formation Top (m)	Formation Bottom (m)	Vertical Thickness (m)	GR (API)	Density (g/cm^3	Rt-den	Fluid - den	Phi (Ø)	Rw	Sw	Hc_sat
	5100	5166									
A	5100	5116	16	65	1.86	202	0.18	0.349	0.327	0.102	0.898
B	5116	5128	12	56	1.84	202	0.18	0.325	0.327	0.143	0.857
C	5128	5132	4	66	1.89	202	0.18	0.312	0.327	0.118	0.882
D	5132	5158	26	62	1.83	202	0.18	0.347	0.327	0.282	0.718
E	5158	5166	8	88	1.92	46	0.18	0.304	0.327	0.3426	0.574
Total			66								

Note :R_w = Resistivity , S_w = water saturation , GR = Gamma ray logs , $H_{c_{sat}}$ = Hydrocarbon saturation

Note: A,B,C,D and E were used to differentiate various reservoirs formation for well-02 for petrophysical parameters computation.

Incompressibility (Lamda-Rho) Versus V_P/V_S

Figure 22 indicates changes of incompressibility (Lamda-Rho) versus V_P/V_S interpreted as sands and shale/sand/shale sequences. This plot aligns close to lamda-rho axis which shows that lamda-rho is a better rock unit (lithology) discriminator . Blackish eclipse indicate shale section, the yellowish indicate saline riched sand (brine) , the red eclipse shows hydrocarbon sand and the blue indicate the gas zone .

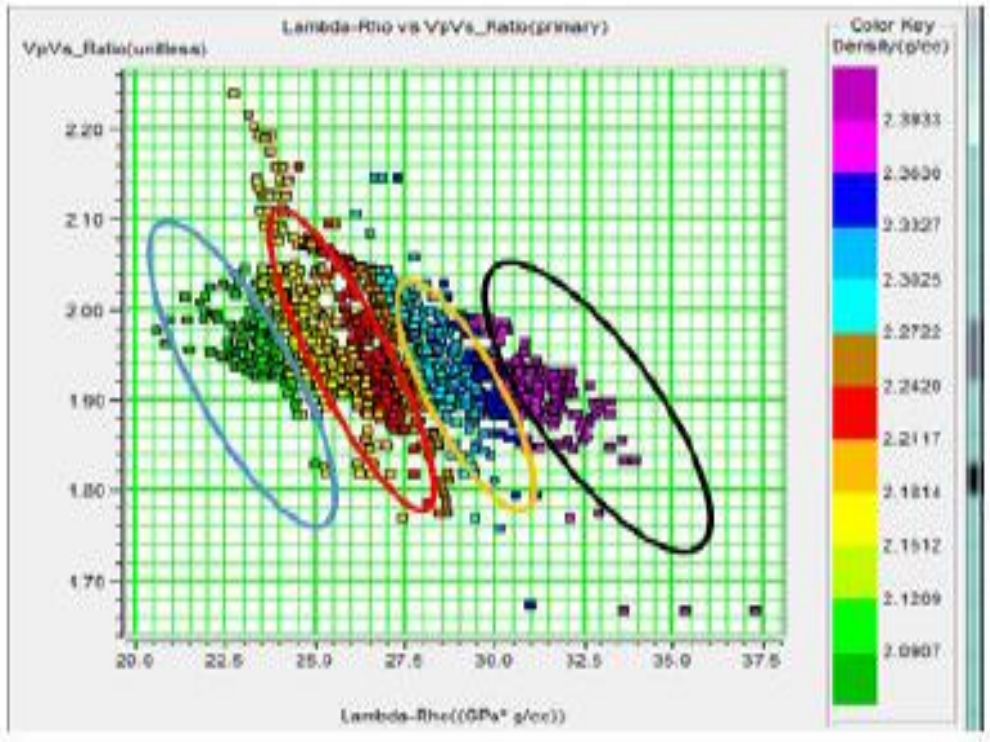

FIG 22: Cross-plot of Lamda – Rho against V_P/V_S black eclipse indicate shale zone, the yellow indicate reservoir water (brine) sand, the red eclipse shows hydrocarbon sand and the blue indicate the gas zone

MU-RHO Against Density

The Mu-Rho versus density crossplot were used to discriminate lithology (rock units). The value of mu-rho is high for sand but low for shale. However the density of shale is higher compared to that of sand. Additionally, water saturated sand (brine) shows higher density than hydrocarbon bearing sand (oil and gas) . Hence , the blue eclipse , figure 23, shows hydrocarbon riched sand, the yellow eclipse indicates the water saturated sand (brine), then the black eclipse indicates the shale region.

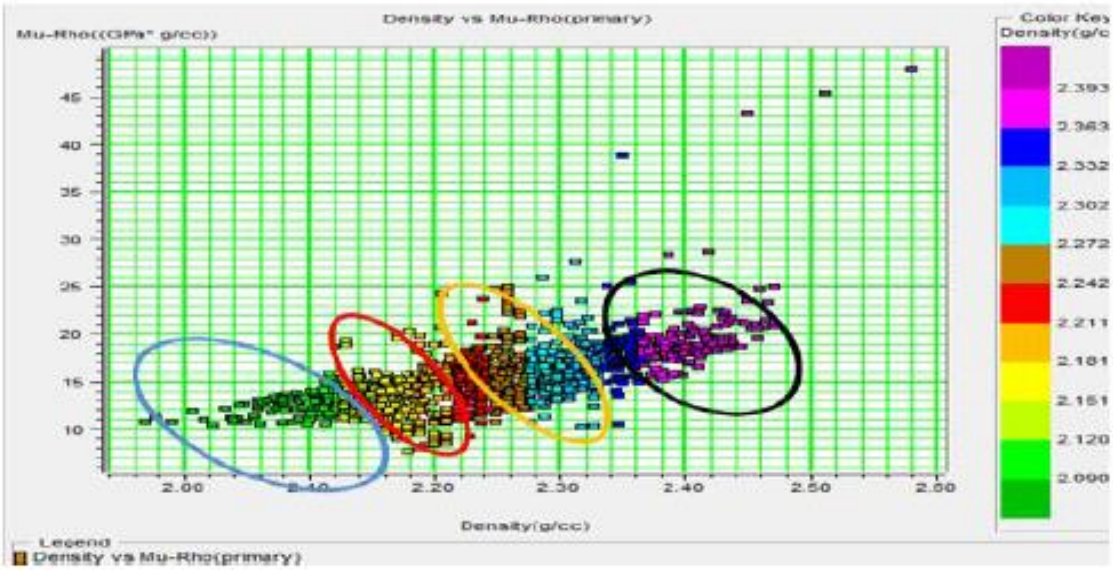

FIG.23: The cross- plot of Mu-Rho versus density (blue eclipse stands for hydrocarbon bearing sands, yellow represent brine saturated region , red stands for brine sand and the black for shale region)

Lamda-Rho (Incompressibility) Against Mu-Rho

Crossplots of lamda rho (λ_p) versus mu-rho (μ_p) in figure 24, shows demarcation into four zones which is inferred into shale (black sphere),water saturated sand (brine)(yellow sphere), oil (red sphere) and gas region (blue sphere) with the least density value. The plots shows the complexity of generating $\lambda\rho$ compared to $\mu\rho$. That magnitude is less for the reservoir sand. Well-02 ,06 and 07 were the logs used for the analysis. Reservoir evaluation were performed on each well to ascertain reservoir parameters using log transform interface called E-log templates inbuilt in the Hampson Russell Software.

Cross plotting selected rock properties and attributes result obtained were as follows:

(a.) V_P/V_S ratio against Acoustic Impedance differentiating the REV-01 reservoir into hydrocarbon zone , brine zone and shale zone.

(b.) Lamda - Rho (incompressibility) versus V_P/V_S discriminated reservoirs into sands and shale/sand/shale sequences.

(a.) Mu-Rho versus density are lithology discriminator, Mu –rho values higher for sand but low in shale. However, shale denser than sand.

(b.) Lastly, the cross- plot of Lamda-Rho (λ_p) versus Mu- rho (μ_p) indicates distinction into four sections which were shale, brine and gas zone evidenced by lowest density values.

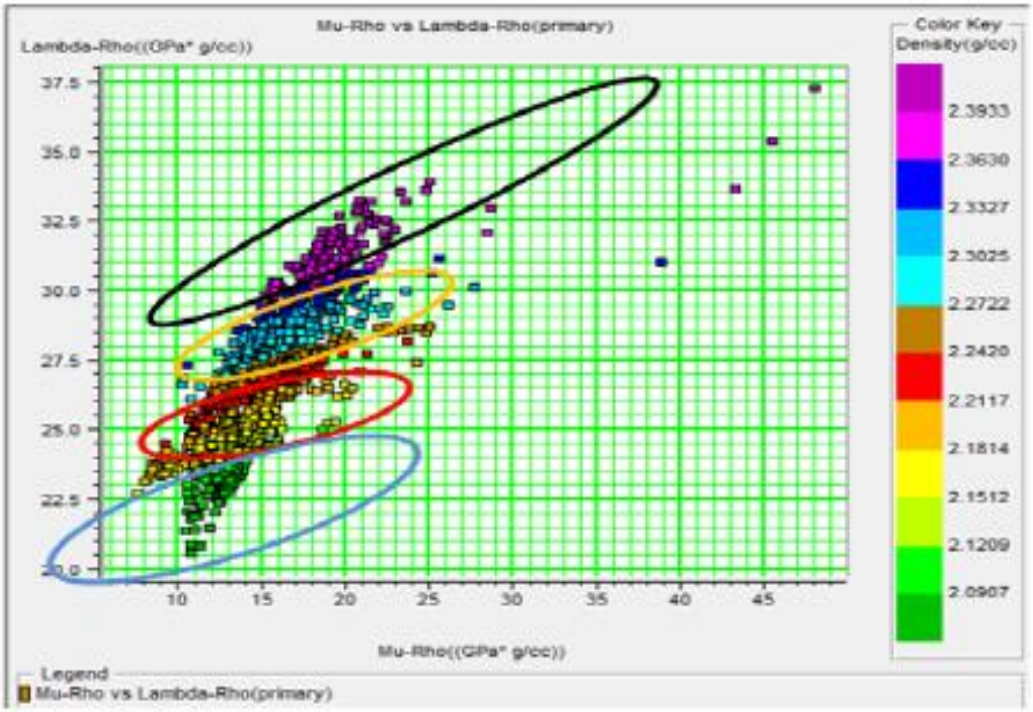

FIG 24: The Crossplots of Lamda-Rho (λ_p) versus Mu-Rho (μ_P) black eclipse stands for shale, yellow eclipse represent brine, red eclipse stand for oil and blue represent gas section.

Formation Evaluation And Petrophysical Analysis Of Result

Quality control

Data adjustment of seismic attributes done on 3-D seismic data (volume) targeted to ascertain how sensitive it is to resolve gas zones at target locations within the wireline logs data.

The gas sands possess high V_p range as 3,082 m/s -3,373 m/s (10,200 ft/s to 10,460 ft/s) Vs range 1982 m/s to 2,267 m/s (6500 ft/s to 7800ft/s) compared to shale 2590 m/s to 3097 m/s (8900 ft/s to 10200 ft/s) .However Vp value is lower than that of the formation beneath named brine sands 3544 m/s to 3920 m/s (11,302 ft/s to 12,550 ft/s), the Vs readings for brine sand, higher than that of gas sands. Highly porous sands characterized by low velocity at both ends were gas sand and brine sand clusters although low porosity (Ø) sands were characterized by high velocity values at both ends. The cut-off porosities were less than 0-38 for sand and greater than 0.38 for shaley formation.

The porosity and the clay content influence the velocity . These two identified reservoirs contains average porosity of 21% .

The clean sandstones intercalated with shale was interpreted as the lithology . The P-wave velocity were used to discriminate lithology . Sonic log was also used as a valid tool for discriminating rock unit (lithology) or fluid contents.

The confirmed ''hard'' sandstones whose P-wave impedance is greater than 22,002 g/cm3 ft/s and Vs above 13,000 g/cm3 ft/s. There exist certain exploration challenges in the data set , namely the discrimination of hydrocarbon bearing sands from shale- sand essentially separation of gas sands from brine –saturated sandstones. Hence , the existence of lithology anomaly shows sands also shale indicated by high gamma ray readings which possess similar acoustic impedance values causing no reflection coefficient near offset seismic section.

From AVO analysis the gas sand was differentiated from sand saturated with saline water (brine) including shale , V_P/V_S versus compressional wave crossplot. Gas saturated sands in well-02 shows increment

in compressional (P) impedance . However the domain of compressional impedance alone cannot delineates the rock types due to the magnitude of transition for the P-impedance values of the lithology.

Due to the nature of shale that it can be harder than sand when underlying an overburden load, here it is characterized by higher pressure and high compaction , hence the compressional wave velocity (V_P) travels through it, faster than in sand therefore higher V_P/V_S domain . Although S-wave responds to variation in fluid type and saturation .

Thus ,V_P/V_S impedance ratios was employed for DHI (direct hydrocarbon indicators) using amplitudes approach. However, cross-plotting V_P/V_S ratio versus P-impedance indicates a different separation between sand and shale . This contrast in V_P/V_S at the sand-shale boundary resulted to changes in reflection amplitude with offset at the lithologic boundary.

From figure 25 P- Impedance versus V_P/V_S cross-plot of various rock type with fluid shows the V_P/V_P ratio from 116-8. Most of the gas sands have V_P/V_S of 1.8 to 2.4 standing for N/G value of 0.9. Thus, very small shale intercalation will cause a great increase in V_P/V_S ratios , compared to uniform clean sands (N/G=1).

Also V_P/V_S domain was reliable in discriminating various rock types. It can be seen that different models, their N/G were 1.00, 0.90.0.80,0.70,0.60 and 0.50. The reduction in N/G affected V_P/V_S ratio increase , irrespective of pore space (porosity), though for high gas saturation in the sands. Avseth et al.,(2006). Note for hydrocarbon sands V_P/V_S range of 1.66- 1.90.

However there exists in the cross-plots, an inverse relationship between porosity and impedance given by the slope of a regression line. Estimate of average porosity of 0.21, for the reservoir sandstones, and discriminated them from the shale and brine sand. P-impedance drops greatly when sands have high porosities but increase slightly when the sands have low porosity.

This is mainly due to the relative contrast to the intercalating shale. The porosity value indicates good reservoirs quality (Figure 25).

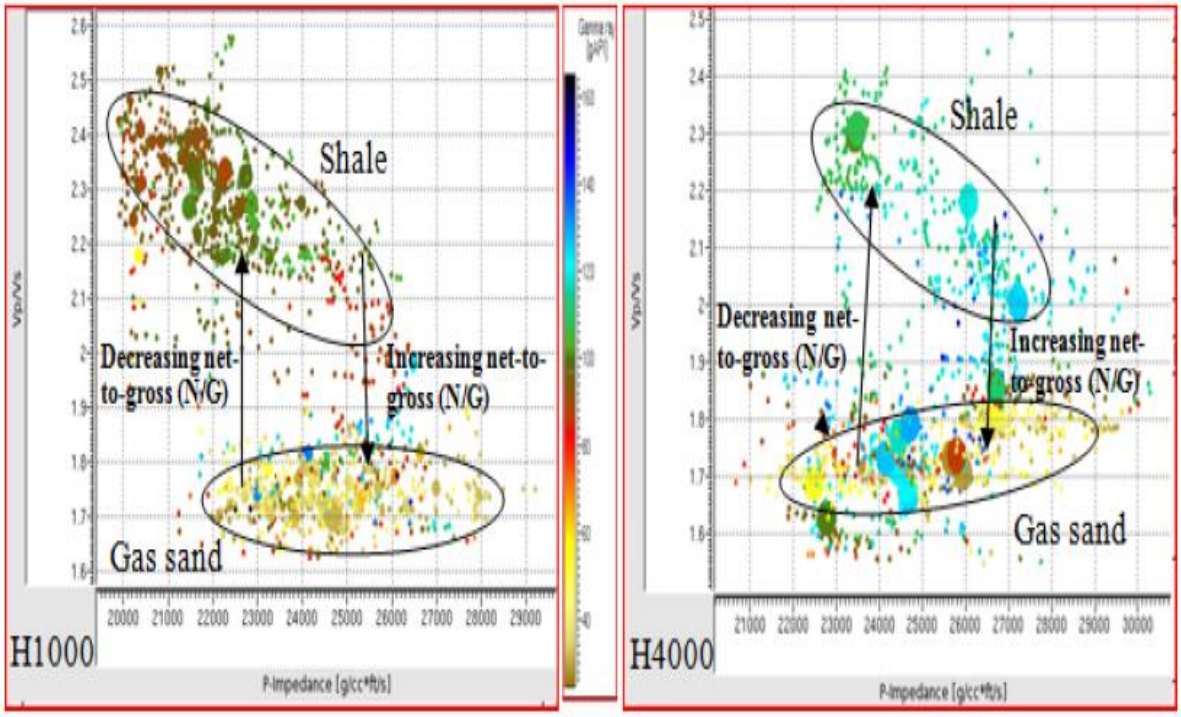

FIG 25.:Cross-plot of P-impedance versus Vp/Vs showing areas of increasing and decreasing N/G for the field.

Data adjustment of seismic attributes done on 3-D seismic data (volume) targeted to ascertain how sensitive it is to resolve gas zones at target locations within the wireline logs data. The sensitivity of seismic attributes must be carried-out as it plays vital role in rock properties response for pore fluid and rock unit (lithology) contrasts for reservoir definition. The difference in rock unit (lithology) and the response of porous formation (reservoir rocks) as regards pore fluids depends on porosity, fluid type and the rock constituents like shale volume intercalated within sandstone. Seismic wave (velocities) propagated through the rock and its density were defined by changes in basic rock properties, certain rock characters namely impedance and elastic moduli ,affects the fundamental rock behaviours. Each rock character behave distinctly or when related to the entire lithology it can be sensitive in property.

Basically , separation of gas zones from well attributes generated , this can be work on seismic volume. In Figure 26, crossplotting compressional wave velocity (V_P) versus shear wave velocity (V_S) within a given gas reservoir intervals used to determine the shale volume (V_{Sh}) . The gamma ray (GR) used to discriminates

lithologies. The fluids contents can be differentiated using V_P and V_S attributes. In the recorded sonic logs, three (3) rocks types were determined which includes: shale, sands saturated with formation water (brine) including gas sands. There were better demarcation shown, for brine sand and gas sands confirming Badrack et al,(2004) findings. The existence of good separation between sand and shale contradicted earlier prediction which lies on the same mudrock line. This implies weak fluid factor exist between brine sand and shale interface , also brine sand and gas sand interface. Strong fluid factor reflection exist between shale and gas sand interface , this was evident in large demarcation for shale and gas sand clusters according to Fatti et al.,(1994).

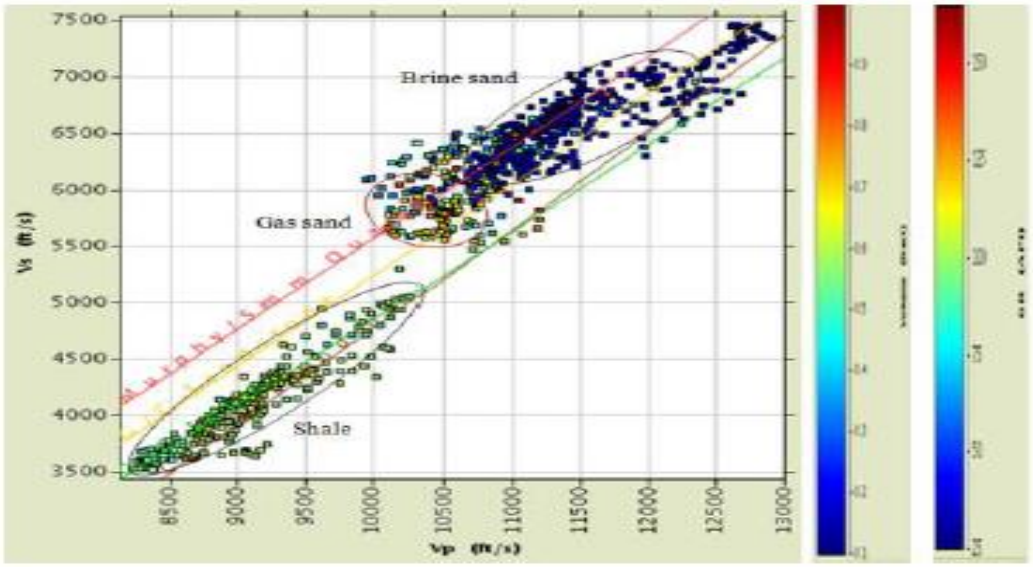

FIG.26:Crossplot of Vs versus Vp to discriminate the brine sand , gas sand and shale

The gas sands possess high V_p range as 3,082 m/s -3,373 m/s (10,200 ft/s to 10,460 ft/s) Vs range 1982 m/s to 2,267 m/s (6500 ft/s to 7800ft/s) compared to shale 2590 m/s to 3097 m/s (8900 ft/s to 10200 ft/s) .However Vp value is lower than that of the formation beneath named brine sands 3544 m/s to 3920 m/s (11,302 ft/s to 12,550 ft/s), the Vs readings for brine sand, higher than that of gas sands. Highly porous sands characterized by low velocity at both ends were gas sand and brine sand clusters although low porosity (Ø) sands were characterized by high velocity values at both ends. The cut-off porosities were less than 0-38 for sand and greater than 0.38 for shaley formation.

Figure 27 V_p and $V_s$were cross-plotted with gamma ray (GR) respectively , colour demarcated. The shale volume (Vsh) estimated ,lithologic units were differentiated on the basis of their velocities. Sand formation characterize with higher P-wave and S-wave velocities. Investigating compressional wave velocity crossplotted with porosity, the P-wave also crossplotted with density, colour demarcated, shown in figure 27, used to discriminate lithology such as sand and shale.

The sands were colour coded ranging from grey ; the texture of the sands were very fine (lower-upper part) , silty , well sorted , and clay possess the qualities such as slightly calcareous, poorly consolidated. The porosity correlates perfectly to gamma ray , the smaller the gamma ray value in (API), the higher its porosity . This gamma ray behavior used to identify lithology and reservoir quality within the field. Therefore, low gamma ray reading indicate low clay contents ,associated with sandstones. However gamma ray with high value delineate high clay content interpreted as shale formation.

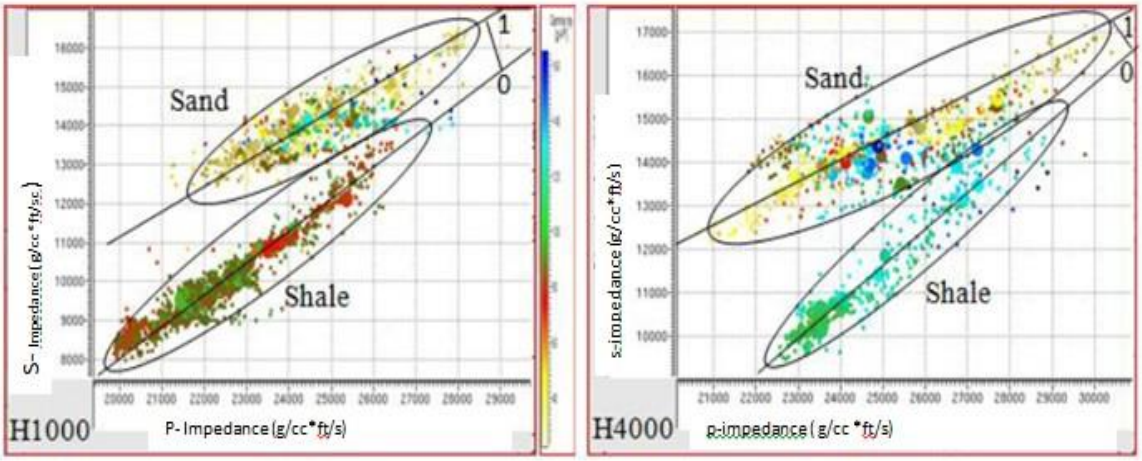

FIG 27: Cross-plot of P-wave Impedance versus s- wave impedance differentiating sand from shale colour coded.

Yellow colour were used to depict sands/low shale contents , whereas green(or red) colour points higher shale contents. The scattered points in figure 27 indicates rocks linked to clay content , affected not only by the compaction of the rock but with pore geometry according to Calderon et al.,(2007).

The porosity and the clay content influence the velocity . These two identified reservoirs contains average porosity of 21%. The clean sandstones intercalated with shale was interpreted as the lithology . The P-wave velocity were used to discriminate lithology . Sonic log was also used as a valid tool for discriminating rock unit (lithology) or fluid contents.

According to the cross-plots using wells data, parameters namely P-wave impedance, P-wave velocity, porosity and volume of shale were insignificant to aid good correlation in the study area. Density log was used to carry-out lithologic correlation (porosity and shale volume) .

Wang (2001) opined that seismic velocities are not affected by bulk density increment. Due to zero offset reflection coefficient, shale - sand interface were weak , the contrast between Vp value for shale and sand were also small, hence poses difficulty in contrast within the medium, hence affecting net-to-gross (N/G).

Therefore the small difference , implies that Vp for sand and shale are similar , hence the phase shift linked to wave travels in sand and shale are the same. Stovast et al.,(2006).

The frequency amount in the reflection are similar . Determining layer characteristic instead of interface properties , inversion of seismic amplitude to acoustic impedance were carried-out.

According to Calderon and Castagna (2007), they opined that " model based inversion seem to be cumbersome inversion method using well log suites (wireline) and SEG-Y seismic data. In the reservoir top, seismic wave, exhibit low contrast in velocity and acoustic impedance aids in predicting lithology.

The wireline log display, can be interpreted interms of P-impedance against S-impedance cross-plot, to understand the behavior of sand with various fluids. Figure shows the cross-plot of P-impedance

versus S-impedance colour coded for gamma rays values. The linear trend analysis was done to identify rock unit shown in figure 42 here the data points are not well scattered. The lithology called gas sand section was displaced towards the lower left side and the water saturated sand unit called brine displayed on the upper right side , thus porous rock formation termed reservoir sands characterized by low density less than that of shale .

The confirmed ‘’hard’’ sandstones whose P-wave impedance is greater than 22,002 g/cm3 ft/s and Vs above 13,000 g/cm3 ft/s. There exist certain exploration challenges in the data set , namely the discrimination of hydrocarbon bearing sands from shale- sand essentially separation of gas sands from brine –saturated sandstones. Hence , the existence of lithology anomaly shows sands also shale indicated by high gamma ray readings which posses similar acoustic impedance values causing no reflection coefficient near offset seismic section.

Hence , the sandstone shows anomaly differentiated by simultaneous inversion of compressional (P-wave) and shear (S-wave) impedances. The cross-plot showing conspicuous petrophysical facies sand whose ends members agreed with ‘NG=0’ to that of shale and gas sand ‘’NG=1’’, for log impedance data.

Hence the link of modeling petrofacies using logs , to classify 3 D seismic inversion, it is important to show majorly the petrophysical categories differentiated using P-impedance from shear wave impedance domain within the specific sections. Interestingly, every petrofacies analysis can be implemented using compressional wave impedance and shear wave impedance within the major reservoir zones. Due to channel sand zones within the reservoir, it is plotted on the hydrocarbon sands trends where V sand=1.

The sands shows an anomaly and can be mistaken with shale since their P-impedance values looks alike. For lithologic interpretation , data integration approach were adopted . The result of the wells and geology of the field shows that brine sands exhibit higher P-impedances values compared to gas sands. Ambiguity expressed in lithology and fluid detection were based on acoustic impedance

, sometimes this can be removed by adding information concerning V_P/V_S attributes at non-normal incidence. Madiba & McMechan (2003), Ostrander (1984), Domenico (1976), Smith & Gidlow (1987).

According to Veeken & Davies (2006) ,attested that the ratio V_P/V_S posited that useful information can be extracted fluid contents, this is link to pore spaces of rocks . However, gas sands indicates low V_P/V_S ratios. Therefore, inverting P-impedance (I_P) and shear –impedance (I_S) zones to V_P/V_S(or I_P/I_S) , to the pore fluids contents , the next step is to separate lithology from the pore fluid impacts.

The pore spaces fitted with water, can be determined by adding up all the water volume component within the pore spaces (the fraction containing movable water, bound water and water entrapped in pores unconnected). The presence of thin bed and mixed lithologies can pose an effect on the cross-plot of P-impedance versus S-impedance , with changes in clay content dispersed by shale and claystone clusters, whereas presence of hydrocarbon saturation and silts intercalated with clay both affects the brine sand and gas sand clusters.

Hence, ,the prevailing condition suggest transitional environment, evident in sand/shale cluster overlapping. Empathically, the acoustic impedance of gas sand and surrounding shale were noted to be equal , hence the sandstone were mistaken for shales, the shale does not have shear details present as emphasized by Roden et al.,(2005), Pendrel and Van (2000).

From AVO analysis the gas sand was differentiated from sand saturated with saline water (brine) including shale , V_P/V_S versus compressional wave crossplot. Gas saturated sands in well-02 shows increment in compressional (P) impedance . However the domain of compressional impedance alone cannot delineates the rock types due to the magnitude of transition for the P-impedance values of the lithology.

Figure 28 , shows that cross-plotting acoustic impedance with V_P/V_Sratio created from the particular zones was based on the well log data. The cross-plot when compared with rock physics interface for

various net-to-gross ratios. This technique followed the methods used by Avseth et al.,(2006). The formation (shale) were selected among the sealing shales above and below the reservoirs. Though the result , somewhat could be erroneous due to the sealing shale which does not in essence equate the interbedded shale found in the reservoirs. Hence, shale usually possess a high V_P/V_S ratio than reservoir sands.

Due to the nature of shale that it can be harder than sand when underlying an overburden load, here it is characterized by higher pressure and high compaction , hence the compressional wave velocity (V_P) travels through it, faster than in sand therefore higher V_P/V_S domain . Although S-wave responds to variation in fluid type and saturation .

Thus ,V_P/V_S impedance ratios was employed for DHI (direct hydrocarbon indicators) using amplitudes approach. However, cross-plotting V_P/V_S ratio versus P-impedance indicates a different separation between sand and shale . This contrast in V_P/V_S at the sand-shale boundary resulted to changes in reflection amplitude with offset at the lithologic boundary.

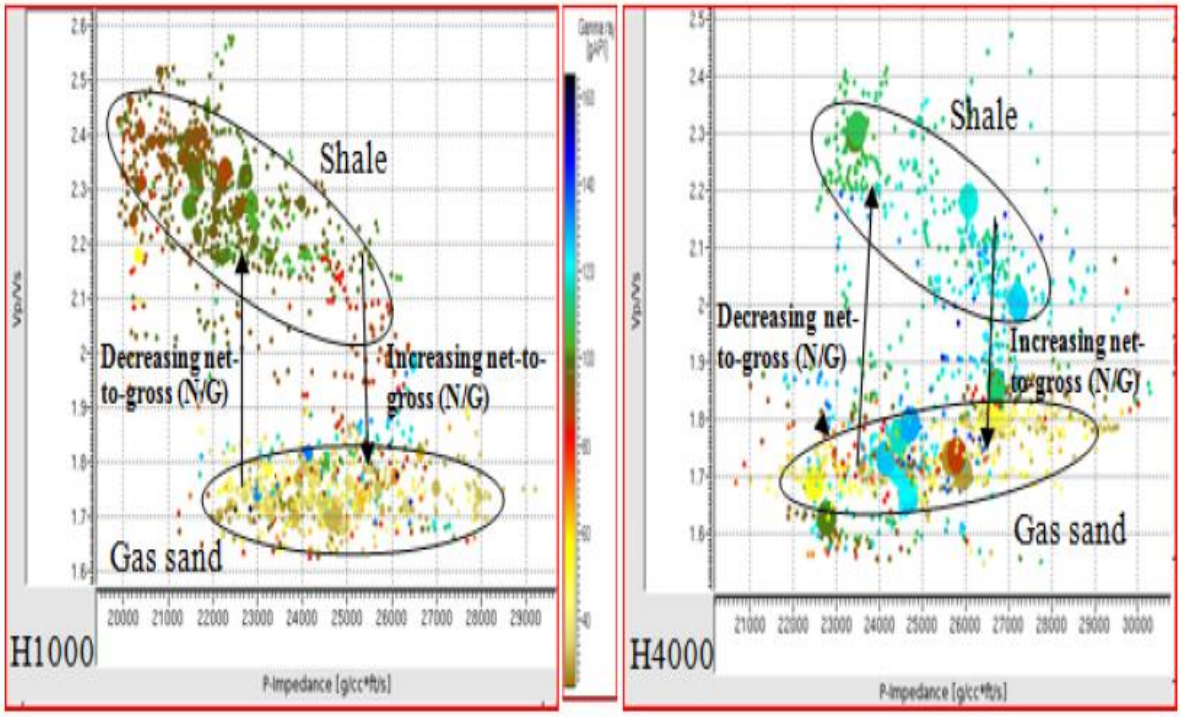

FIG.28:Cross-plot of P-impedance versus Vp/Vs showing areas of increasing and decreasing N/G for the field.

From figure 28 P- Impedance versus V_P/V_S cross-plot of various rock type with fluid shows the V_P/V_P ratio from 116-8. Most of the gas sands have V_P/V_S of 1.8 to 2.2 standing for N/G value of 0.9. Thus, very small shale intercalation will cause a great increase in V_P/V_S ratios , compared to uniform clean sands (N/G=1). Also V_P/V_S domain was reliable in discriminating various rock types. It can be seen that different models, their N/G were 1.00, 0.90.0.80,0.70,0.60 and 0.50. The reduction in N/G affected V_P/V_S ratio increase , irrespective of pore space (porosity), though for high gas saturation in the sands. Avseth et al.,(2006). Note for hydrocarbon sands V_P/V_S range of 1.66-1.90.

The N/G values assisted in ascertaining anisotropy of sands , this shows the sand fraction ,permeable sand compared to the entire reservoir and sands reservoirs with intercalated shales (impermeable). Consequently , N/G depends on scale . A reservoir portion with high N/G using well log scale could be low in N/G using seismic scale according to Avseth et al.,(2009). Hence , reduction in N/G leads to great increment in V_P/V_S and very little shale intercalations influence a great increase in V_P/V_S. Clean sands (N/G=1) containing 100 percent gas. The sand zones which contains sealing shales at some intervals the gas saturated sand range of V_P/V_S ratios about 2.0, this value depict brine sands. The observable patchy saturation pattern . Hydrocarbon sands have V_P/V_S ratios spans 1.7 to 1.9 this sand was saturated with gas. This separates shales clearly. As shown in Figure 28..

Thus, the rock physics templates of AI versus V_P/V_S produce in Table 6 was employed to classify porosity, satu8ration including net-to-gross (N/G) using well log suite also with elastic inverted result. This was pointed out by Avseth et al.,(2006).

The AI (acoustic impedance) generated from seismic inversion plots against porosity was gotten from density log. , this was cross-plotted as shown in figure 44 to link between porosity and AI (acoustic impedance). Three categories were obtained : low to high impedance values and very low porosity value indicating shale. Secondly, high impedance and high porosity (sand intercalated with shale), and the last being high impedance and high porosity depicting sands. However, in the

cross-plots an inverse relationship exist between porosity and impedance as given by the slope of it regression line. Estimate of porosity value (average) as 0.23, depicting sandstone reservoir , this was differentiated from the shale and brine sand, there was a drop in impedance (P-wave) as it was noticed that sand were made up of high porosities which increased slowly. The slow increase was motivated by relative contrasts in shale intercalation .This porosity value shows good reservoir quality. The P- impedance against porosity cross-plot (Figure 29) indicate that H1000.0 and H4000.0,shows that porosity relates to P-impedance inversely this plot was colour coded using gamma ray and water saturation can be used for simultaneous interpretation or classification of porosity, saturation and the N/G from well log data as well as elastic inversion results. This was pointed out by Avseth et al. (2006).

The acoustic impedance derived from Seismic inversion versus porosity derived from density log was cross-plotted in Figure 29 to show the link between porosity and acoustic impedance. This shows three main trends: one for relatively low to high impedance and low porosity (shale), another for relatively high impedance and high porosity (clayey or shaly sand), and the third for high impedance and high porosity (sand). However there exists in the cross-plots, an inverse relationship between porosity and impedance given by the slope of a regression line. Estimate of average porosity of 0.21, for the reservoir sandstones, and discriminated them from the shale and brine sand. P-impedance drops greatly when sands have high porosities but increase slightly when the sands have low porosity. This is mainly due to the relative contrast to the intercalating shale. The porosity value indicates good reservoirs quality. Figure 29 P-impedance versus porosity cross-plot for H1000 and H4000, colour coded to gamma ray and water saturation. porosity shows an inverse relation with p-impedance.

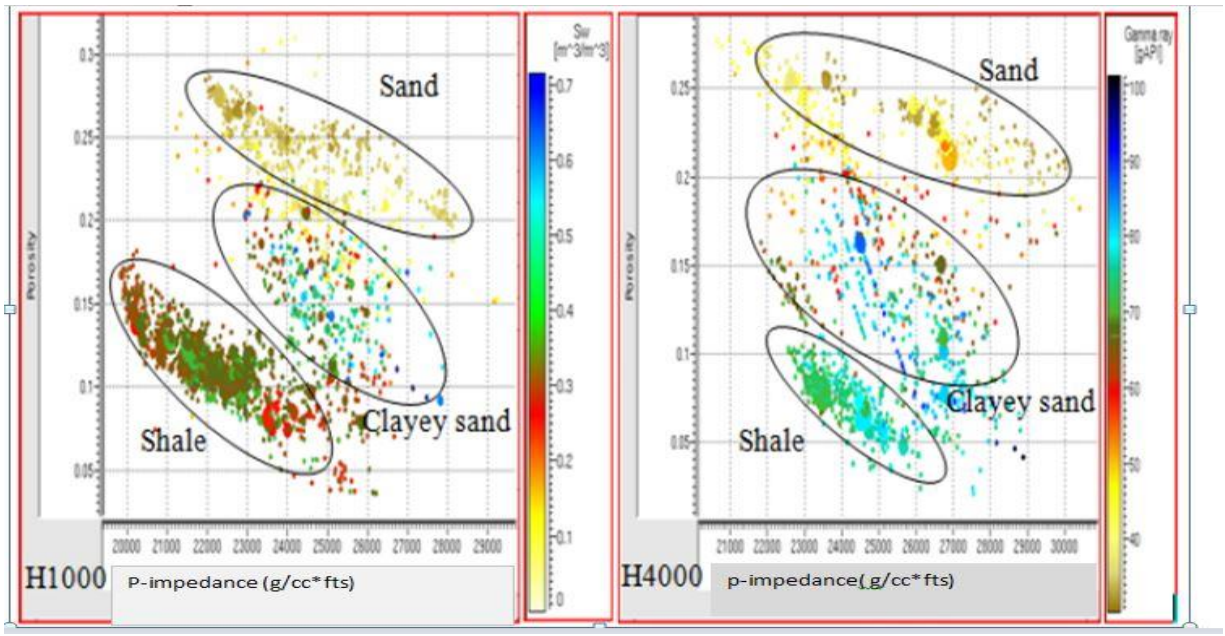

FIG.29. Plot impedance(P-wave) against porosity for H1000.0 and H4000.0 ,showing relationship between porosity and impedance (inversely related) colour coded with gamma ray and water saturation.

From the well log data the crossplot of P-impedance versus gamma ray, colour coded , to resistivity and water saturation as indicated in Figure 30. Establishing the relation of P-impedance with rock properties for a targeted sections, applying a frequency values of interest for the inversion. The outcome shows that lithology can be differentiated in gamma ray space. In H1000.0 the gamma ray reads low value also P-impedance reads high value interpreted as hydrocarbon bearing sands within this section . There is a clear distinction between the sand and shale as expressed in the gamma ray log.

High P-impedance , high resistivity with low gamma ray indicate hydrocarbon \sand. Based on the outcome of inverting AVO, Lame's moduli (μ) and lamda (λ) were obtained , confirmed in the work published by Goodway, Chen & Downtown (1997), where the combined density (ρ),μ and λ, this was from the well logs and were obtained, the component $\mu\rho$ and Lamda-Rho ($\lambda\ \rho$) were vital in differentiating sand quality and fluid contact. These two parameters Mu-Rho is called the rigidity ($\mu\rho$) and Lamda-Rho is called the incompressibility ($\lambda\ \rho$) that assisted in further interpreting for AVO response.

The crossplot of P-wave velocity shows a discrimination between lithology, gas sand and shale. In enhancing this delineation , density and compressional wave , colour coded to gamma ray readings, density versus P-wave velocity were cross-plotted indicating lithofacies namely shale and sand.(Figure 31).

Gas not necessarily influenced rigidity even if it is presence in sand , however sand have high rigidity ,hence the outcome shows high contrast between incompressibility and rigidity as seen in $\lambda\ \rho - \mu\rho$ domain in Figure 31 below. The sands contains water saturation (0.01-0.22) but shales have water saturation between (0.23-0.55) indicating poorly consolidated sediments.

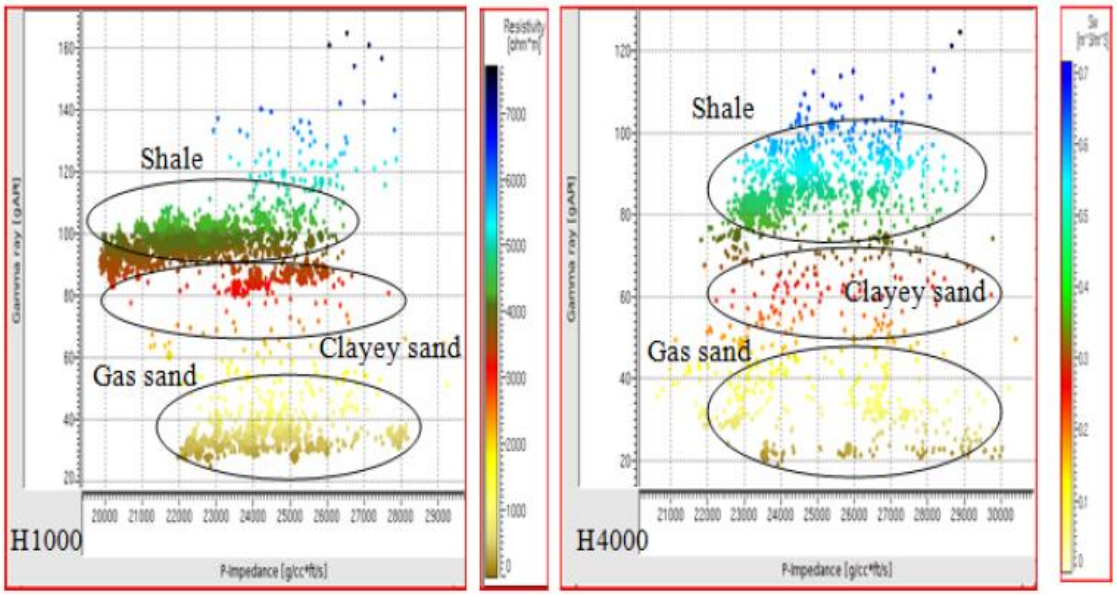

FIG.30: P- impedance and gamma ray cross-plot, differentiating fluids and lithologies- P-impedance and resistivity noted to be high, gamma ray reads low for hydrocarbons sands.

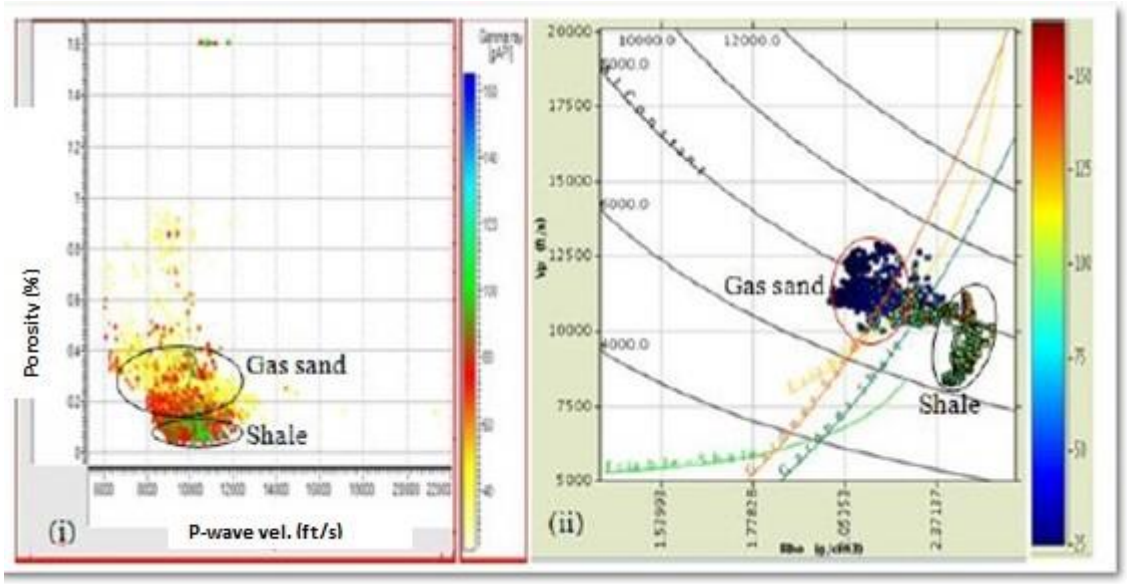

FIG31 :Crossplot showing (i.) compressional wave velocity (P-wave) versus porosity (%). (ii.) Density against compressional wave velocity (P-wave) , colour coded to gamma ray, green colour stands for shales, blue and yellow stands for sand shales shows higher density ,Vp measured in ft/s and Rho(ρ) is the bulk density (g/ft3).

Figure 32 Lamda – Rho and mu-Rho cross-plot, H1000.0 and H4000.0.,After analyzing logs , it shows good distinction between sandstone and shales indicated high rigidity . On the crossplot of $\lambda\rho$ versus $\mu\rho$ fluid can be discriminated . Based on theory $\lambda\rho$ and $\mu\rho$ are perpendicular . P-impedance (Ip) and S-impedance (IS). The clear cut resolution of gas sand was well shown in $\lambda\rho$ and $\mu\rho$ domain , where low$\lambda\rho$ depict better contrast between sand and shale . The least $\lambda\rho$ value (incompressibility versus density) indicates best gas sand values, also $\mu\rho$(rigidity X density) indicates higher shales values. $\lambda\rho$ versus $\mu\rho$ cross-plot gives a great merit in isolating both lithology and gas sections. The gas sands anomaly found in the upper left side quadrant with lowest $\mu\rho$ was interpreted as shale whereas more pronounced lithologies such as slits , cemented shales plotted on the opposite right hand quadrant on the upper side interpreted as shale.

Comparing Figure 32 with Figure 33 shows a better improved separation, this is because $\lambda\rho$ versus $\mu\rho$ axes are orthogonal according to Lame's parameters or moduli, when compared to compressional wave (P-impoedance) against shear wave (S-impedance) cross-plot gave rise to clear discrimination. Identification of gas sand using $\lambda\rho$ and $\mu\rho$ domain according to Goodway et al.,(1998) was proved successfully.

In Figure 48 , we noticed that both $\mu\rho$(Mu-Rho) and V_P/V_S spaces can differentiate lithologic fluids within the area , high $\mu\rho$ and low V_P/V_S(1.90) shows gas sand while higher V_P/V_S (1.90-2.50) value shows shale. The gamma ray signature interpreted as good discriminator for rock unit and reservoir quality in the field.

Plotting reflection coefficient against angle of incident (θ)using wireline well log data as illustrated in Figure 34, reservoir named H1000.0 indicated sands interpreted as class llp, also H4000.0 indicates class ll showing no phase reversal . The two reservoirs (H1000.0 and H4000.0) sands has higher velocity overlain by shale ; negative reflectivity whose value increased with offset evident.

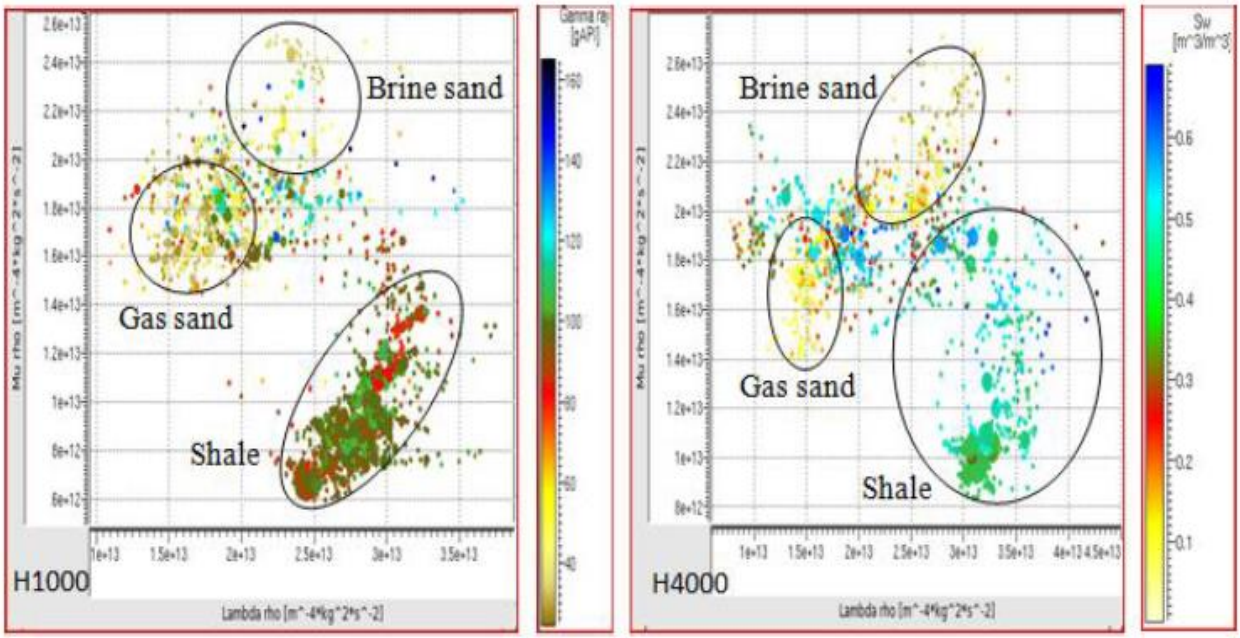
Brine sand
Gas sand
Shale
H1000
Lambda rho [m^-4*kg^2*s^-2]
Mu rho [m^-4*kg^2*s^-2]
Gamma ray [gAPI]
Brine sand
Gas sand
Shale
H4000
Lambda rho [m^-4*kg^2*s^-2]
Mu rho [m^-4*kg^2*s^-2]
Sw [m^3/m^3]

FIG 32 Cross-plot of Lamda rho versus Mu Rho for H1000.0 and H4000.0, colour (coded) gamma ray- Sw values. The log analysed suggest good discrimination, sandstone and shales discriminated based on rigidity , here high rigidity differentiated sandstones from shales.

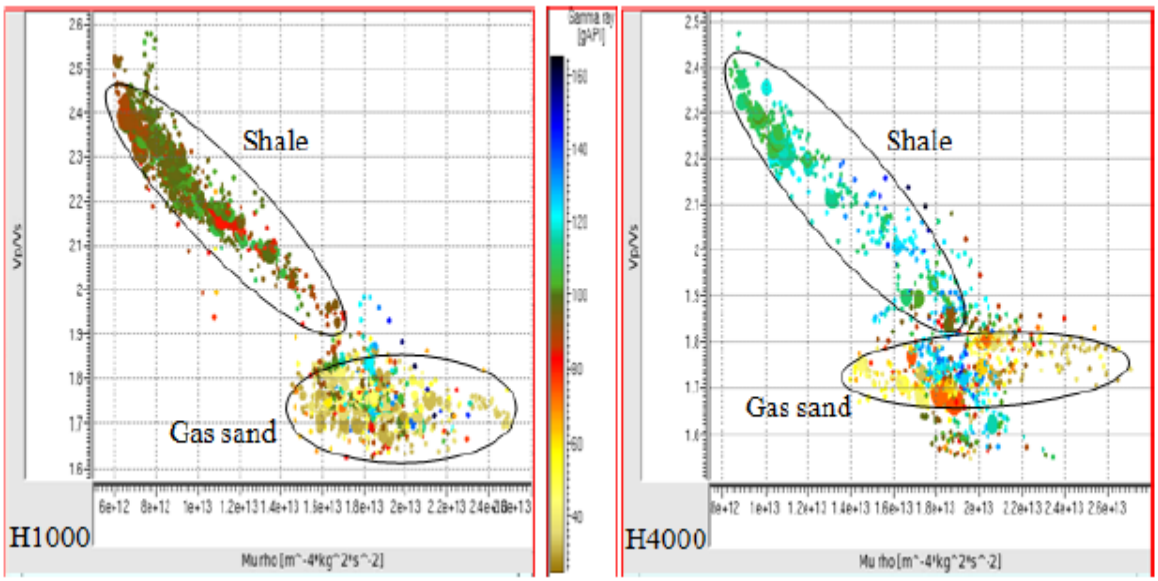

FIG 33:Cross-plot of Mu-Rho versus Vp/Vs for reservoir depicted H1000.0 and H4000.0, colour (coded) with gamma ray .

H4000.0 Sand shows low thus negative slope, hence, zero polarity contrast while H1000.0 sand shows weak but positive intercept but negative gradient initiating polarity contrast with offset. These anomalies represents sand filled with hydrocarbons characterized by weak normal incident contrast when likened to capping shale. Hence petrophysical characteristics establish correlation between reservoir behavior which includes pore spaces (porosity) gas sands saturated with clastics.

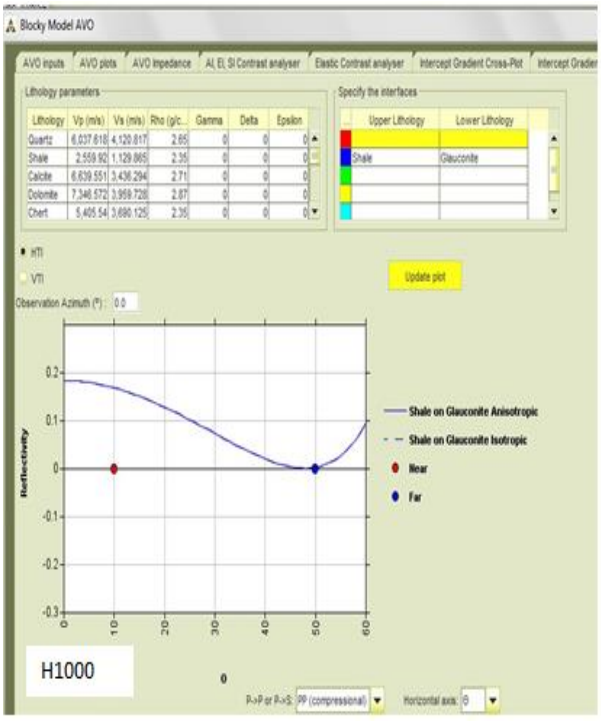
Blocky Model AVO
AVO inputs
AVO plots
AVO impedance
AI, EI, SI Contrast analyser
Elastic Contrast analyser
Intercept Gradient Cross-Plot
Lithology parameters
Specify the interfaces
Upper Lithology
Lower Lithology
Shale
Glauconite
HTI
VTI
Update plot
Observation Azimuth (°):
Reflectivity
Shale on Glauconite Anisotropic
Shale on Glauconite Isotropic
Near
Far
H1000

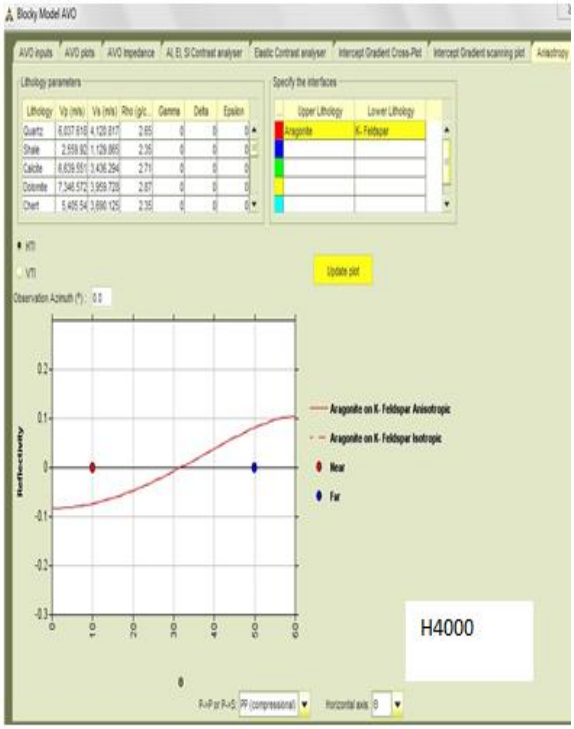
Blocky Model AVO
AVO inputs
AVO plots
AVO impedance
AI, EI, SI Contrast analyser
Elastic Contrast analyser
Intercept Gradient Cross-Plot
Intercept Gradient scanning plot
Anisotropy
Lithology parameters
Specify the interfaces
Upper Lithology
Lower Lithology
Aragonite
K- Feldspar
HTI
VTI
Update plot
Observation Azimuth (°):
Reflectivity
Aragonite on K- Feldspar Anisotropic
Aragonite on K- Feldspar Isotropic
Near
Far
H4000

FIG 34: Cross-plot of Reflection coefficient Vs. incident angle (θ) for H1000.0 Incident angle angles were estimated from CMP gather employing RMS velocities gotten from sampled NMO correction . The angle of incident (θ) labeled on the abscissa . Amplitudes normalized for each trace.

CONCLUSION AND RECOMMENDATION

Conclusion

For Exploration and production of hydrocarbons to be achievable it is necessary to characterize the hydrocarbon reservoir correctly in terms of its fluid properties and lithology. Thus, good knowledge of petrophysical parameters must be known to understand the lithology and fluid content.

The Acoustic Impedance (Zp), Lamda-rho (λρ), Mu-rho (μρ), Poisson impedance (PI), shear impedance (SI), Extended impedance (EI), Two – term elastic impedance (EI2), Extended elastic impedance (EEI) P-wave modulus, Shear modulus, Bulk modulus, Young modulus, Poisson ratio, Lame coefficient, Lame's Coefficient/Shear modulus, Shear modulus *Rho (mu-Rho) attributes were found to be highly useful in lithology and fluid discrimination within the reservoir in the crossplot analysis. The λ-μ-ρ technique was useful in identifying gas sand , due to the demarcation in responses of both the λρ and μρ sections to gas sands versus shale . Many different lithologies were also identified by the crossplot of λρ versus μρ. This was possible because various rock unit properties response differently due to its fluid content and mineral properties. We used mu-Rho and V_p/V_s to discriminate, sandstone and shale based on its rigidity. This was used to discriminate sandstone from shales.

We show that high μρ and low $\frac{V_p}{V_s}$ (1.8) show gas sand while higher $\frac{V_p}{V_s}$ (1.8 – 2.4) value shows shale. The sand found here had low water saturation values (0.0 – 0.20) while shale had higher water saturation (0.22 – 0.50) showing that sediments were poorly consolidated.

We were able to combined density (ρ), μ and λ, from wells logs to differentiate sand quality and fluid contact using parameters like mu-rho (μρ) and Lamda – Rho (λρ).

The mu- Rho called rigidity (μρ) and Lamda- Rho is incompressibility. The Acoustic impedance was high based on the data for all lithologies. The rigidity found in the area was high based on the mu-Rho result obtained.

Recommendation

The challenges for AVO analysis at present lies on the quality of data made available .

Company's policy of confidentiality have gone beyond bounds. Today allots of researchers are willing to devote their time for AVO studies but company help in frustrating their effort by not releasing the needed data useful for this work.

The following are recommendation for this study;

(1.) More scientist should re-channel their effort from more theoretical studies to more applications , from P-wave Seismic data to multicomponent seismic data.

(2.) Further studies of AVO should be done in other areas of Niger Delta like deep and ultra deep regions of the basin.

(3.) Much researches should be done on the interpretation of the 3 D seismic data especially P-wave impedance and S- wave impedance inversion for gas saturation , net- to- gross and porosity determination for other oil field to reduce drilling risk , hence enhancing field's production capacity.

REFERENCES

Aki, K. & Richards, P.G. (2002). *Quantitative Seismology*, University Science Books, 2nd Edition, 123-144, Editor: Jane Ellis, ISBN: 0-935702-96-2, Maple-Vail Book Manufacturing Group.

Avseth, P., Jorstad, A. , Alart-Jan, V. & Mavko, G.(2009). Rock physics estimation of cement volume , sorting and net-to- gross in North sea sandstone . *The Leading Edge*,*28*(1), 98-108.

Avseth, P., Wijngaarden, A.J., Mavko, G. & Johansen, J. (2006) Combined porosity saturation and net-to-gross estimation from rock physics templates: Ann. Meeting, New Orleans, *SEG Technical Program Expanded Abstracts*,*25*,1856-1860.

Bachrach, R., Beller, M.,Liu, C.C., Perdomo, J.,Shelander , D., Dutta, N. & Benabentos , M.(2004). Combining rock physics analysis , full waveform Prestack inversion and high resolution seismic interpretation to map lithology unit in deep water a Gulf of Mexico case study. *The Leading Edge*, *23*(4),378-383.

Bortfeld, R., (1961). Approximation to the reflection and transmission coefficients of plane longitudinal and transverse waves. *Geophysical Prospecting*, 9, 485-503.

Calderon, J.E., & Castagna, J. (2007) Porosity and lithologic estimation using rock physics and multi-attribute transforms in Balcon Field, Colombia. *Society of Exploration Geophysics*,*26*(2),142-150

Castagna,J.P.,Batzle,M.L.& Eastwood ,R.L.(1985). Relationship between compressional and shear – wave in elastic silicate rocks. Geophysics, 50, p.571-581.

Calderon, J.E., & Castagna, J. (2007) Porosity and lithologic estimation using rock physics and multi-attribute transforms in Balcon Field, Colombia. *Society of Exploration Geophysics*,*26*(2),142-150

Castagna, J.P., Swan , H.W & Foster, D.J. (1998) Framework for AVO gradient and Intercept Interpretation. *Jour. Geophys.* 63(3), 948-956.

Domenico, S.N. (1976) Effect of brine-gas mixture on velocity in an unconsolidated sand reservoir. *Geophysics*, *41*,882-894.

Ehinola, O.A. & Ejeh,I.O. (2009). Basic geometry and sedimentary fill modeling of parts of onshore Niger Delta , Kuwait. *Journal of Science Engineering*,*36*,147-163.

Evamy, B.D., Herebourne, J., Kameling, P., Knap, G.A., Molley, F.A., & Rowlands, P.H. (1978). Hydrocarbon Habitat of Tertiary Niger Delta. *American Association Petroleum Geologist.* Bulletin. *62*,1-39

Fatti, J.L., Smith, G.C., Vail, P.J. & Levitt , P.R (1994) . Detection of gas sandstone reservoirs using AVO analysis : A 3D seismic case History using the geostack technique. *Geophysics, 59,*1362-1376.

Feng,H & Bancroft,J.C(2006) . AVO principles, processing and Inversion. *CREWES Research Report, 18,* 1-19.

Foster, D.,Smith, S.W., Dey- Sarkar, S.K. & Swan, H.W (1993). A closer look at hydrocarbon indicators, 63 rd SEG. Meeting Washington ,D.C.,USA, *Expanded Abstract,*731-733.

Goodway, B., Chen, T ,& Downton, J., (1997). Improved AVO fluid detection and lithology discrimination using Lame petrophysical parameters; λp, μρ, & λμ fluid stack., from P and S inversions . *67th CSEG National Convention . Expanded Abstracts*;22(7) 3-5.

Koefoed, O. (1955). On the effect of Poisson's ratios of rock strata on the reflection coefficients of plane waves. *Geophysical Prospecting,*3, 381-387.

Knott, C.G., (1899). Reflection and refraction of elastic waves with seismological applications.*Phil. Mag*., 48, 64-97.

Madiba, G.B. & McMechan(2003) Processing , Inversion and Interpretation of a 2D Seismic data set from the North Viking Graben . *North Sea, 68(*3), 837-848.

Ostrander, W.J. (1984) .Plane – wave reflection coefficients for gas sand at nonnormal angles of incidence. *Geophysics, 49,*1637- 1648.

Ostrander, W.J., (1982). Plane – wave reflection coefficients for gas sands at non-normal angles of incidence. *Geophysics*, 49, 1637-1648.

Pendrel ,J. & Stewart, R. R(2000). Estimation and Interpretation of P and S Impedance – volumes from Simultaneous Inversion of P-wave offset Seismic data . *Society Of Exploration Geophysics, Expanded Abstrac*t, OnePetro, 1-4. DOI:10.1190/1.1815683, https:// www.researchgate.net/publication/2288327162288.accessed.pdf.06 October,2021.

Reijers, T.J.A (1996) Selected Chapters on Geology 6 Sedimentary Geology and Sequence Stratigraphy in Nigeria and Three Case Studies and a field Guide.197

Roden,R.,Castagna,J. & Jones, G.(2005). The impact of prestack data phase on the AVO Interpretation Workflow – a case study . *The Leading Edge, 24*(9), 890-895.

Roden,R., Forrest, M. & Holeywell,R.(2005) The impact of Seismic Amplitudes on prospect Risk Analysis, Business Briefing :E&P. The Oil and Gas Review Issue.

Ross, P.C. (2000). Effective AVO crossplot modeling : A tutorial,. Geophys. 65,700-711.

Rosa, A.L.R.(1976). Extraction of elastic parameters using seismic reflection amplitude with offset variation . M.Sc Thesis , Univ. of Houston .

Rutherford, S.R & Williams, R.H (1989).Amplitude – versus – offset variations in gas sands *Jour*. *Geophys*, 54 (6),680-688.

Rutherford, S.R & Williams, R.H (1989).Amplitude – versus – offset variations in gas sands. *Journal Geophysics*, *54* (6), 680-688.

Shuey, R.T., (1985). A simplification of the Zoeppritz equations: *Geophysics*, 50, 609-614

Smith, G.C. & Gidlow, P.M., (1987). Weighted stacking for rock property estimation and detection of gas. *Geophysical Prospecting*, *35*,993 – 1014.

Smith, J.C. & Sutherland, R.A. (1996) . The fluid factor as an AVO Indicator. *Geophysics*, *61*,1425-1428 .http://doi.org/10.1190/1.1444067.

Stovas, A., Landro, M. & Avseth, P. (2006) AVO attribute Inversion for finely layered reservoirs. *Geophysics, 71* (3) ,25-36.

Veeken, P.C.H., Rauch, M.,Gallardo, R., Guzman, E. & Villasenor, R. (2002) . Seismic Inversion of the Fortuna National 3D survey, Tabasco, Mexico, First Break 20,257-294.

Veeken, P.C.(2007). *Seismic stratigraphy, Basin Analysis and Reservoir characterization*. Handbook of Geophysical Exploration. Elsevier, Klaus Helbig and Sven Treitel (Eds.), Amsterdam, Boston . ISBN : 9780080453118.

Veeken, P.C.(2007). Seismic stratigraphy, Basin Analysis and Reservoir characterization. Handbook of Geopohysical Exploration. Elsevier, Klaus Helbig and Sven Treitel, 37(1), 528, Amstewrdam, Boston . ISBN : 9780080453118.

Zoeppritz, K. (1919). Erdbedenwellen VlllB, On the reflection and propagation of seismic waves. *Góttinger Nachrichten*, 1, 66- 84.

Wang, Y. (1999) . Approximation to the Zoeppritz equations and their use in AVO analysis . *Geophysics*, *64*,678-690.